FORSCHUNGSZENTRUM KARLSRUHE

T e c h n i k u n d U m w e l t

Wissenschaftliche Berichte

FZKA 6191

Comparison of AGASA Data with CORSIKA Simulations

M. Nagano[1], *D. Heck, K. Shinozaki*[a], *N. Inoue*[a] *and J. Knapp*[b]

Institut für Kernphysik

[1] permanent address: 11-401, 5-8 Higashi, Hasuda, Saitama, Japan,
e-mail: <mnagano@icrr.u-tokyo.ac.jp>
[a] Department of Physics, Saitama University, Urawa 338, Japan
[b] Department of Physics and Astronomy, University of Leeds, Leeds LS2 9JT, United Kingdom

Forschungszentrum Karlsruhe GmbH, Karlsruhe
1998

Abstract

Comparison of AGASA Data with CORSIKA Simulations

An interpretation of AGASA data by comparing the experimental results with the simulated ones by CORSIKA has been made. General features of the electromagnetic component and low energy muons observed by AGASA can be well reproduced by CORSIKA. There are some discrepancies between them, which must be studied in more detail to understand. In the following some simulation results related to the AGASA experiment are summarized.

The form of the lateral distribution of charged particles agrees well with the experimental one between a few hundred m to 2000 m from the core, irrespective of the hadronic interaction model (QGSJET or SIBYLL) and the primary composition (proton or iron). It doesn't depend on the primary energy between $10^{17.5}$ and 10^{20} eV as the experiment shows.

If we evaluate the particle density measured by scintillators of 5 cm thickness as S(600) by taking into account the similar conditions as in the experiment, the conversion relation from S(600) to the primary energy will be written as

$$E(eV) = (2.95 \pm 0.20) \times 10^{18} \left(\frac{S(600)}{14.25} \right)^{1.015 \pm 0.010} .$$

within 10 % uncertainty among the models used and composition, which suggests the present AGASA conversion factor is the lower limit.

Though the form of the muon lateral distribution fits well to the experiment within 1000 m from the core, the absolute values change with hadronic interaction model and primary composition. The slope of the $\rho_\mu(600)$ (muon density above 1 GeV at 600 m from the core) vs. S(600) relation in experiment is flatter than that in simulation of any hadronic model and primary composition. Since the slope seems to be constant from KASCADE ($\sim 10^{15}$ eV) to AGASA energies ($\sim 10^{19}$ eV), we need to study this relation in a wide primary energy range.

There is a disagreement of the attenuation length of S(600) determined by AGASA and that by CORSIKA simulation. We need further study not only evaluation of simulation data, but also redetermination of experimental values with accumulated data at the highest energy region.

Zusammenfassung

Vergleich von AGASA Daten mit CORSIKA Simulationsrechnungen

Eine Interpretation von AGASA Daten durch Vergleich der experimentellen Resultate mit Daten von CORSIKA Simulationen wurde vorgenommen. Allgemeine Eigenschaften der elektromagnetischen Komponente und der niederenergetischen Muonen, wie sie vom AGASA Experiment beobachtet werden, können gut von CORSIKA reproduziert werden. Allerdings gibt es auch einige Unterschiede, die noch näher untersucht werden müssen, um verstanden zu werden. Im folgenden werden einige Simulationsergebnisse, die sich auf das AGASA Experiment beziehen, zusammengefaßt.

Im Abstandsbereich zwischen einigen 100 m bis zu 2000 m vom Schauercore stimmt die Form der Lateralverteilung der geladenen Teilchen gut mit der experimentellen Form überein, unabhängig vom verwendeten hadronischen Wechselwirkungsmodell (QGSJET oder SIBYLL) und von der Zusammensetzung der Primärteilchen (Proton oder Eisen). Im Energiebereich zwischen $10^{17.5}$ und 10^{20} eV hängt sie nicht von der Primärenergie ab, wie das Experiment zeigt.

Wenn wir die mit Szintillatoren von 5 cm Dicke gemessene Teilchendichte als S(600) auswerten, wobei wir ähnliche Bedingungen wie im Experiment betrachten, dann kann die Beziehung zwischen S(600) und der Primärenergie geschrieben werden als

$$E(eV) = (2.95 \pm 0.20) \times 10^{18} \left(\frac{S(600)}{14.25} \right)^{1.015 \pm 0.010} ,$$

mit einer 10 % Unsicherheit, die von den verwendeten Modellen und der Zusammensetzung herrührt, was nahelegt, daß der gegenwärtige AGASA Umrechnungsfaktor die untere Grenze darstellt.

Obwohl im Bereich bis zu 1000 m Core-Abstand die Form der Muon-Lateralverteilung gut mit dem Experiment übereinstimmt, ändern sich die Absolutwerte in Abhängigkeit vom Wechselwirkungsmodell und von der primaeren Zusammensetzung. Die Steigung von $\rho_\mu(600)$ (Muon Dichte oberhalb von 1 GeV bei 600 m Core-Abstand) als Funktion von S(600) ist im Experiment flacher als in den Simulationsrechnungen, unabhängig vom hadronischen Wechselwirkungsmodell und der Primär-Zusammensetzung. Da diese Steigung vom KASCADE Experiment ($\sim 10^{15}$ eV) bis zu AGASA-Energien ($\sim 10^{19}$ eV) konstant zu sein scheint, müssen wir diese Funktion in einem weiten Bereich der Primärenergie untersuchen.

Es gibt eine Diskrepanz in den Abschwächungslängen von S(600), die von AGASA und von CORSIKA-Simulationen ermittelt werden. Daher müssen wir nicht nur die Auswertung der simulierten Daten weiter untersuchen, sondern auch die experimentellen Werte der gesammelten Daten bei den höchsten Energien neu ermitteln.

Contents

1 Introduction **1**

2 AGASA data **5**
2.1 Density measured by scintillation detectors on surface 5
2.2 Muons measured by proportional counters under the absorber 5

3 CORSIKA **6**

4 Results **6**
4.1 Comparison with NKG function 6
4.2 Lateral distibution of electrons, photons and muons 8
4.2.1 Energy dependence 11
4.2.2 Hadronic model dependence 13
4.2.3 Primary composition dependence 13
4.3 Muon lateral distributions with different cutoff energies 13
4.3.1 Primary energy dependence of $\rho_\mu(600)$ 13
4.4 Charged particle densisy, S(600) 16
4.4.1 Energy dependence 16
4.4.2 Fluctuations 18
4.5 Zenith angle dependence of charged particles 19

5 Discussion **23**
5.1 Definition of density used in Akeno/AGASA experiment 24
5.2 Densities measured by scintillator of 5 cm thickness 25
5.3 Primary energy and S(600) relation evaluated by CORSIKA 27
5.4 Composition from muon component 29
5.5 Attenuation of S(600) with zenith angle and the implication on the primary composition around 10^{19} eV 32

6 Conclusion **34**

Acknowledgment **35**

Bibliography **36**

1 Introduction

After the observation of cosmic rays with energies greatly exceeding the Greisen-Zatsepin-Kuzmin (GZK) cutoff energy [1] by the Fly's Eye [2] and the Akeno Giant Air Shower Array (AGASA) [3], six events exceeding 10^{20} eV have been reported by the AGASA group [4].

In order to estimate the primary energy of giant air showers observed by the AGASA, the particle density at a distance of 600 m from the shower axis ($S_0(600)$, suffix 0 denotes the vertically incident shower) is used, which is known to be a good energy estimator [5]. The conversion factor from $S_0(600)$ [per m^2] to primary energy (E_0 [eV]) at Akeno level is derived by simulation [6] based on COSMOS program by Kasahara [7] with the QCDjet model [8] and the relation

$$E_0 = 2.0 \times 10^{17} \times S_0(600)^{1.0} \tag{1}$$

is used. This relation holds within 20 % independent of primary composition and interaction models used [6]. The deviation of the energy spectrum determined in this way from that determined by the 1 km^2 array at Akeno is about 10 % higher in energy around 10^{18} eV as shown in [9]. That is,

$$E_0 = 1.8 \times 10^{17} \times S_0(600)^{1.0}$$

must be applied instead of Eq. (1) in order to be in agreement with that from the lower energy region.

The AGASA energy spectrum in the highest energy region, which is adjusted to the one of the 1 km^2 array at Akeno[1] are compared with the spectra from the Haverah Park [10], the Yakutsk [11] and the stereo Fly's Eye [12] experiments in Fig. 1. All four spectra agree with each other within $\pm$15% in energy. It should be noted that the energy assignment in each experiment has been done separately by each group. The Fly's Eye experiment measures the longitudinal development of electrons above the observation level and is calorimetric. The Yakutsk group determined the energy conversion relation experimentally by measuring not only the lateral distributions of electrons and muons but also the energy loss of electrons above the observation level from the Čerenkov lateral distribution at the observation level. The Haverah Park experiment used water Čerenkov detectors and the AGASA uses plastic scintillation detectors, the energy conversions of both experiments rely on different simulation codes. However, the energy assignment is in fairly good agreement as shown by the water tank experiment at Akeno [13].

On the other hand, Cronin [14] argued that the AGASA energy spectrum should be about 30 % higher in energy, if the energy is assigned in each experiment according

[1] The spectrum determined between $10^{14.5}$ eV and 10^{19} eV using the arrays with different detector spacing at Akeno fits very well with extrapolation of those obtained from direct measurement on balloons and satellites, and with the Tibet result obtained through the observation of the shower at the height of its maximum development. Therefore the AGASA spectrum may be better to normalize to the spectrum by 1 km^2 array.

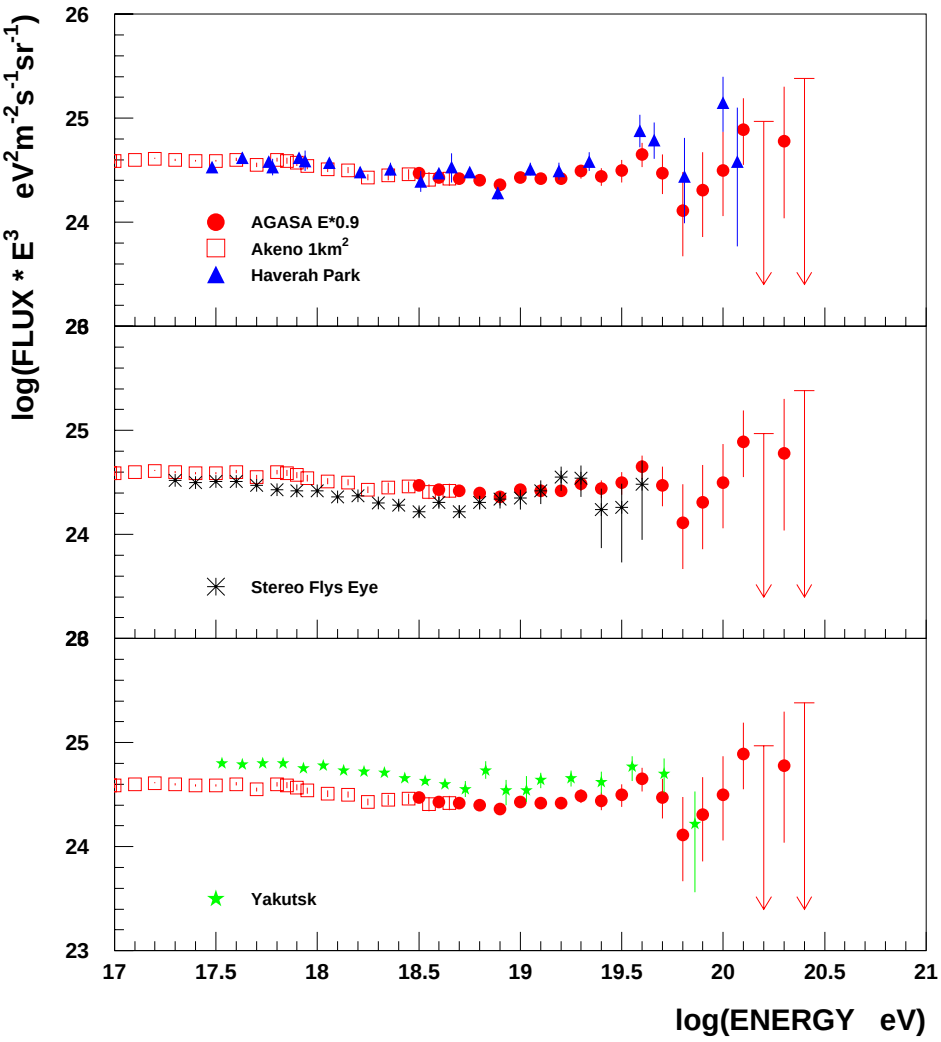

Figure 1: *Energy spectra from the Haverah Park, Yakutsk, stereo Fly's Eye experiments are compared with that from the AGASA experiments.*

to the simulation results based on the MOCCA program with the SIBYLL hadronic interaction model. According to their simulation, the relation should be

$$E_0 = 3.0 \times 10^{17} \times S_0(600)^{1.0}$$

at Akeno level. That is, the AGASA energy spectrum results in much higher intensity than other experiments at the same energy.
Recently Kutter pointed out that the difference is due to the large contribution of low energy photons [15] in the scintillators in case of AGASA. Though the energy loss of electrons and photons in scintillator (ρ_{sc}) in units of a vertically traversing muon is independent of scintillator thickness, the ratio of ρ_{sc} to the number of charged

particles ($R_{sc/ch}$) depends on the core distance. $R_{sc/ch}$ is about 1.1 within 100 m from the core and agrees with the experiment [18], however, it increases as the core distance increases. It becomes about 1.2 around 600 m from the core in case of MOCCA (SIBYLL) and 1.4 in case of CORSIKA (QGSJET) simulations. The difference between the simulation code is due to the difference of energy spectra of low energy photons and electrons far from the core. This ratio $R_{sc/ch}$ depends also on the number of charged particles which increases as the cutoff energy of electromagnetic component decreases.

Therefore, it is quite important to evaluate the energy conversion factor Eq.(1) used in AGASA experiment with other simulation program than the COSMOS simulation, by taking into account the energy losses of low energy photons and electrons in scintillator.

Since the total number of muons in an extensive air shower with a fixed primary energy depends on the chemical composition, the possibility of discriminating heavy particles from protons has been extensively studied by many authors. For example, Dawson et al. [16] argues that the muon density at 600 m from the core ($\rho_\mu(600)$) vs. energy relation observed at Akeno can be consistently explained by the change of composition from heavy around $10^{17.5}$ eV to light around 10^{19} eV which is claimed by the Fly's Eye group [17]. However, they avoided the discussion of change of composition around $10^{17.5}$ eV which is a point of disagreement between the Fly's Eye experiment and the Akeno experiment. According to their simulation result [16], the Fly's Eye data shows 100 % iron below $10^{17.5}$ eV and AGASA data shows heavier than iron below 10^{17} eV.

It is important not only to examine the simulation results with other hadronic interaction models, but also to examine the experimental relation of $\rho_\mu(600)$ vs. S(600) in the lower energy region, e.g. by KASCADE, whether there is any change of slope in the relation.

Since the arrival directions of observed EAS are inclined from the zenith, it is necessary to convert $S_\theta(600)$, where θ represents the zenith angle, to $S_0(600)$. For zenith angles less than 45° ($sec\ \theta \sim 1.4$),

$$S_\theta(600) = S_0(600) exp\left[-\frac{X_0}{\Lambda_{att}}(sec\ \theta - 1)\right] \tag{2}$$

is used, where the attenuation length Λ_{att}=500 g cm^{-2} and X_0 is the atmospheric depth at Akeno (920 g cm^{-2}) [19]. The attenuation of S(600) can be determined from integral $S_\theta(600)$ spectra at various θ by assuming $S_\theta(600)$ at constant intensity in different zenith angles from primaries of similar energy. Fig. 2 shows the variation of S(600) derived using this method of equi-intensity cuts on $S_\theta(600)$ spectra in various zenith angles [20]. The energies of the plots correspond to 40, 20, 10, 5 and 2 $\times 10^{18}$ eV, respectively. A dashed line represents the attenuation (Eq. (2)) used up to zenith angles 45°. The solid lines are represented by

$$S_\theta(600) = S_0(600) exp\left[-\frac{X_0}{\Lambda_1}(sec\ \theta - 1) - \frac{X_0}{\Lambda_2}(sec\ \theta - 1)^2\right] \tag{3}$$

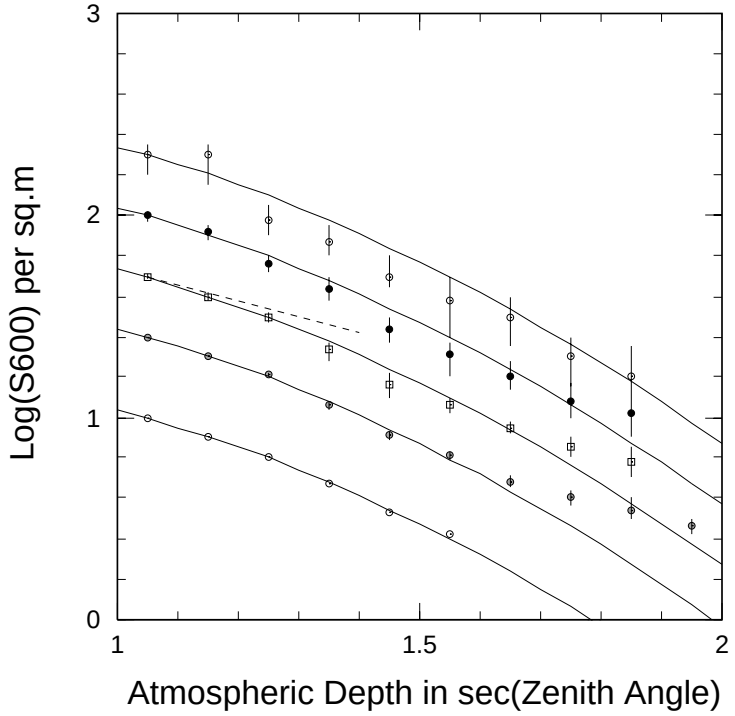

Figure 2: *The variation of S(600) with zenith angle obtained using the method of equi-intensity cuts on the observed $S_\theta(600)$ spectra. Points correspond to 40, 20, 10, 5 and 2 $\times 10^{18}$ eV from top to bottom, respectively. Solid curves are from Eq. (3) and a dashed line from Eq. (2) which was used up to sec $\theta = 1.41$ (45°) so far.*

where Λ_1=Λ_{att}=500 g cm^{-2} and Λ_2=594 g cm^{-2} which was derived in [21]. Though there is a slight discrepancy between data and Eq. (3) for energies above 10^{19} eV, Eq. (3) nearly holds up to *sec* $\theta = 1.7$ between 2×10^{18} eV and 5×10^{19} eV.

Since this relation is related closely to properties of hadronic interactions at ultra-high energy and composition of primary cosmic rays, the interpretation of the present result by simulation result is quite important.

In this report, we use the EAS simulation program CORSIKA (COsmic Ray SImulation for KASCADE) [22] which was developed at Karlsruhe and is now widely distributed and used in cosmic ray research. In CORSIKA several hadronic interaction models are available and comparisons of available interaction models have been done up to 10^{17} eV [23] by the authors and by various experiments from TeV gamma-rays to the highest energy region. Recently the program was improved in simulation technique to be effectively used at the highest observed energy [24]. By employing the effective thin sampling procedure, the computing time is considerably reduced and hence various combinations of simulation conditions with different energies have been realized in this study.

2 AGASA data

2.1 Density measured by scintillation detectors on surface

The AGASA is the Akeno Giant Air Shower Array covering over 100 km^2 area in operation at the village Akeno about 130 km west of Tokyo, in order to study extremely high energy cosmic rays (EHECR) above 10^{19} eV [25, 26].
The lateral distribution of electrons and the shower front structure far from the core are important to determine $S_\theta(600)$ and it is determined with many detectors of 1 km^2 array (A1) by using showers hitting inside the Akeno Branch. The density at core distance r is expressed by the function as

$$\rho = N_e C_e R^{-\alpha}(1+R)^{-(\eta-\alpha)}\left(1.0+\left(\frac{r}{1000}\right)^2\right)^{-0.6}, \tag{4}$$

where $R = r/R_M$, C_e is a normalization factor and R_M is a Molière unit (MU) at height of two radiation lengths above the Akeno level (91.6 m at Akeno) [21]. A fixed value of $\alpha = 1.2$ is used and η is expressed as

$$\eta = 3.97 - 1.79(sec\ \theta - 1). \tag{5}$$

Recently this function is found to be valid up to 3000 m from the core and the highest observed energy $\sim 10^{20}$ eV [27]. It is quite important to examine with simulation whether such energy *independence* can be understood with proton primary composition.

2.2 Muons measured by proportional counters under the absorber

At AGASA muons of energies above 0.5 GeV are measured under the lead+iron or concrete shielding. At the first stage of AGASA experiment, the lateral distribution of muons far from the core was determined with eight muon detectors of 25 m^2 each (threshold muon energy : 1 GeV) in the central part of the Akeno Observatory triggered by the AGASA scintillation detectors on the surface. The lateral distribution of muons above 1 GeV is experessed by the following equation [28].

$$\rho_\mu = N_\mu\left(\frac{C_\mu}{R_o^2}\right)R^{-0.75}(1+R)^{-2.52}\left(1.0+\left(\frac{r}{800}\right)^3\right)^{-0.6}, \tag{6}$$

where N_μ is a total number of muons and $R = r/R_o$. C_μ is a normalization factor and R_o is a characteristic distance and is expressed by the following equation as a function of zenith angle θ.

$$log(R_o) = (0.58 \pm 0.04)(sec\ \theta - 1) + (2.39 \pm 0.05). \tag{7}$$

This formula can be applied up to 3000 m from the core for the showers above 3×10^{19} eV as shown in Doi et al. [29], though the experimental error is still larger than $\pm$50 % beyond 1000 m from the core in the highest observed energy region. To combine the AGASA data of threshold energy of 0.5 GeV with Eq.(6) of 1 GeV threshold, the AGASA data is reduced by a factor 1.4, which is determined at 600 m from the core, in the whole distance range[30]. This factor is now being measured experimentally, but not yet available.

3 CORSIKA

CORSIKA is a simulaton code developed at Karlsruhe [22] and is now widely distributed and used in cosmic ray research. In CORSIKA five high energy hadronic interaction models are available and a comparison of available interaction models has been done up to 10^{17} eV [23]. Among those models QGSJET [31], which include minijet production in hadronic interaction, may be the best to extrapolate to the highest observed energy range. SIBYLL [32] based on the QCD minijet model is also tried in a part of the analysis to compare with other simulation results. Recently the simulation code of CORSIKA was upgraded (v5.62) to accomodate the simulation of air showers at the highest observed energy region [24].

In order to see the general aspects of the simulation results at the highest energy region, simulations with different interaction models (QGSJET, SIBYLL), primary energies ($10^{17.5}, 10^{18.0}$, $10^{18.5}, 10^{19.0}$, $10^{19.5}, 10^{20.0}$ eV), primary masses (proton, iron), thinning levels (10^{-5}, 10^{-6}), zenith angles (0°, 29.6°($sec\ \theta = 1.15$), 39.7°(1.30), and 51.3°(1.60)), and cutoff energies of electromagnetic component (1.0 MeV, 0.1 MeV, 0.05 MeV) have been performed. Cutoff energies of hadrons and muons are fixed in this series of simulation at 100 MeV and 10 MeV, respectively.
In each combination, 10 showers are simulated and the average values at Akeno level are summarized. In order to study fluctuation, 30 showers are used with a thinning level of $10^{-6.5}$ for a limited combinations of conditions.
In the following all simulation results are from CORSIKA, unless otherwise noted.

4 Results

4.1 Comparison with NKG function

In deriving Eq. (1) in Dai et al. [6], the secondary particles are followed until their energy decreases to $E_{th}=10^{-5}E_0$, where E_0 is the primary energy. For particles with $E<E_{th}$, the so-called thin sampling method [33] is applied. Every electron and photon below E_{th} generates a subshower with the NKG function [34] with MU calculated for two radiation lengths above the observation level, which is best fitted to the experimental data at Akeno level.

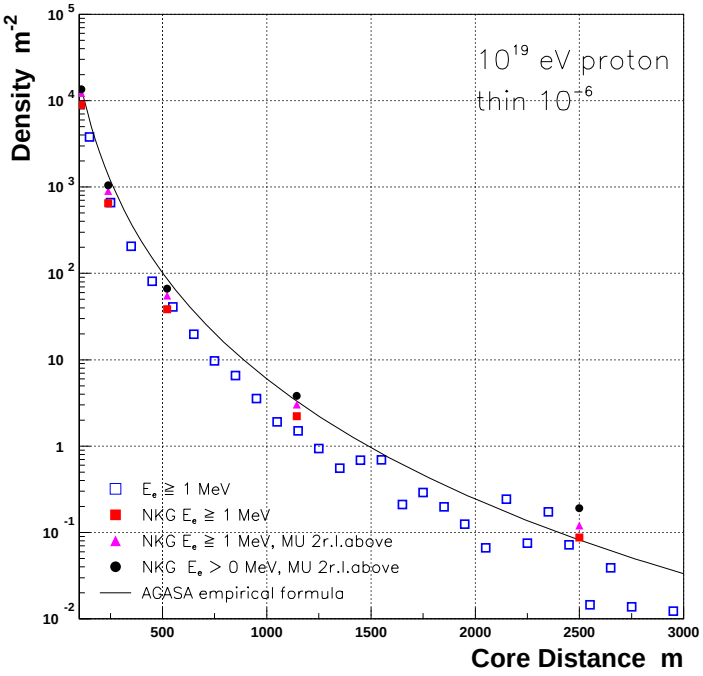

Figure 3: *Electron lateral distribution with a full Monte Carlo simulation is compared with the case where the NKG option is selected in CORSIKA with the QGSJET model. A solid line is the emprical function of AGASA experiment. The simulation by Dai et al.[6] without cutoff energy of electrons and photons and with MU of 2 radiation lengths above the observation level nearly fits to the AGASA emprical formula within 1000 m from the core and should be compared with the solid circles.*

In CORSIKA the electron lateral distribution is also determined with adding subshowers whose lateral distributions represent the analytical form of NKG function with a modification of the cutoff energies of electromagnetic component, if the NKG option is selected. The result of the NKG option is compared with a full Monte Carlo result in Fig. 3. Cutoff energies of electrons and photons are 1.0 MeV in both cases. The agreement between the three dimensional simulation result plotted by open squares and the two dimensinal one plotted by closed squares is good except for large distance from the core (2500 m).

In order to compare the present result with that by Dai et al. the difference of cutoff energy and MU must be taken into account. If we use MU at 2 radiation lengths above the observation level, the density at 523 m from the core increases by 45 %. By applying zero cutoff energy in addition to the change of MU, the density increases about 75 %.

Therefore if we apply the similar method of Dai et al. in CORSIKA and use the same cutoff energy and MU, the density at 600 m from the core is 45 m^{-2} for 10^{19} eV

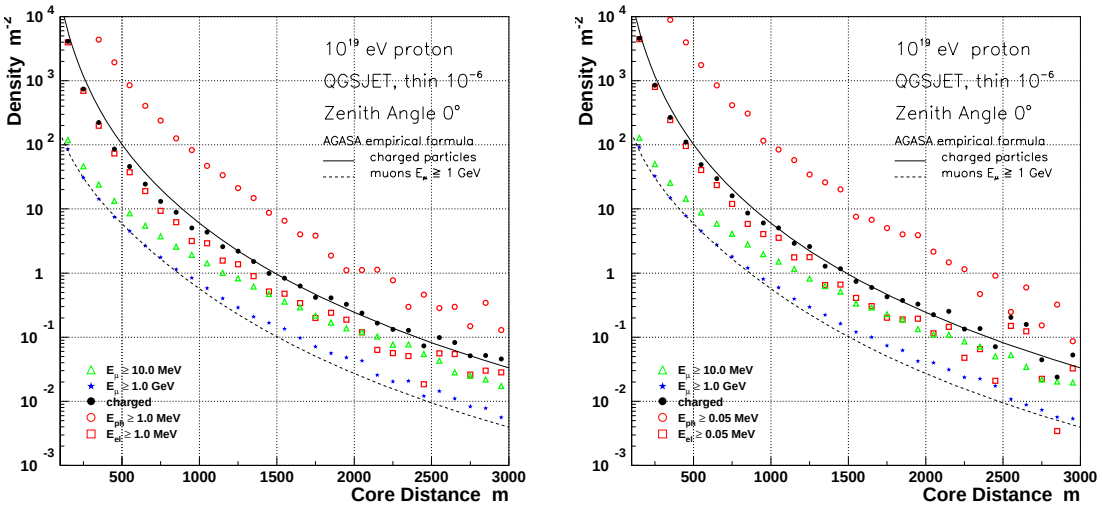

Figure 4: *The lateral distributions of photons, electrons, muons above 10 MeV and 1 GeV simulated with the QGSJET model. Charged particles which are addition of electrons and muons above 10 MeV are also plotted. Thinning level is 10^{-6} and the cutoff energies of photons and electrons are 1.0 MeV (left) and 0.05 MeV (right), respectively. Solid and dashed lines are the AGASA empirical formula on the surface (Eq. (4)) and under absorber (Eq. (6)), respectively.*

and is about 10 % smaller than the value of Dai et al. [6]. That is,

$$E_0 = 2.22 \times 10^{17} \times S_0(600)^{1.0} \tag{8}$$

is derived, if we determine the primary energy vs. $S_0(600)$ relation from the NKG option of CORSIKA under similar conditions of Dai et al. [6].

4.2 Lateral distibution of electrons, photons and muons

The average lateral distributions of photons, electrons and muons do not depend on the thinning levels between 10^{-5} and 10^{-6}, however, thinning levels lower than 10^{-6} are required to discuss the detailed behavior of scintillator response far from the core taking into account the energy spectrum of individual particles, which will be discussed in Section 5.

In Fig. 4, the lateral distributions of electrons, photons and muons (>10 MeV and >1 GeV) are compared with two different cutoff energies of the electromagnetic component, 1.0 MeV and 0.05 MeV. The charged particles (adding electrons and muons above the cutoff energy) are also plotted to compare with the experimental data. Though there are increases in the number of electrons and photons with decreasing cutoff energy (about 10 $\sim$ 20 % [2] for the cutoff energies between 1.0 MeV and

[2]The fraction depends on the primary composition and the hadronic interaction model used.

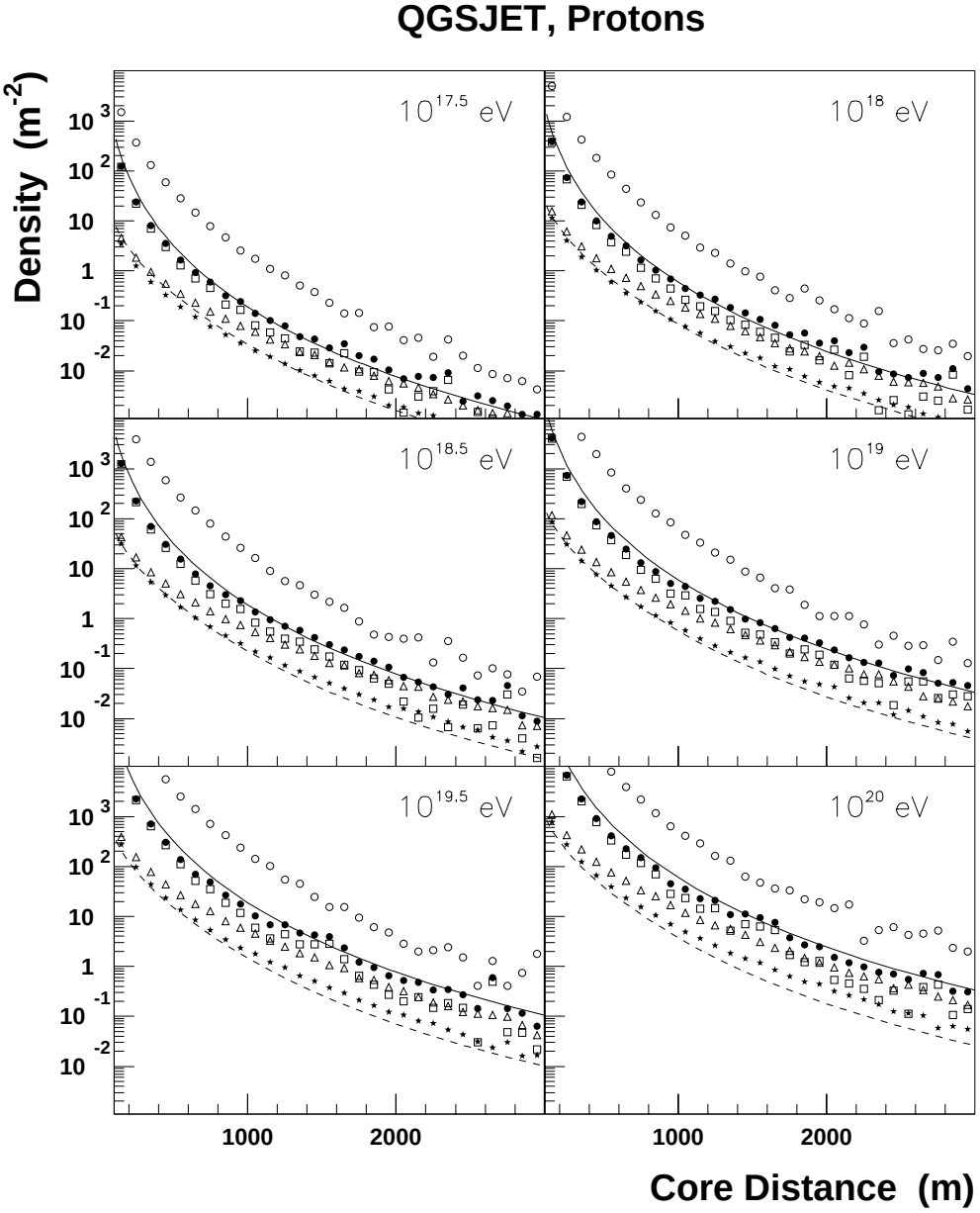

Figure 5: *The lateral distributions of photons, electrons, muons above 10 MeV and* 1 *GeV and charged particles simulated with the QGSJET model. The thinning level is* 10^{-6} *and the cutoff energy for muons is 10 MeV and those for photons and electrons are 1.0 MeV. The solid and dashed lines, and the symbols are the same as in the previous figures.*

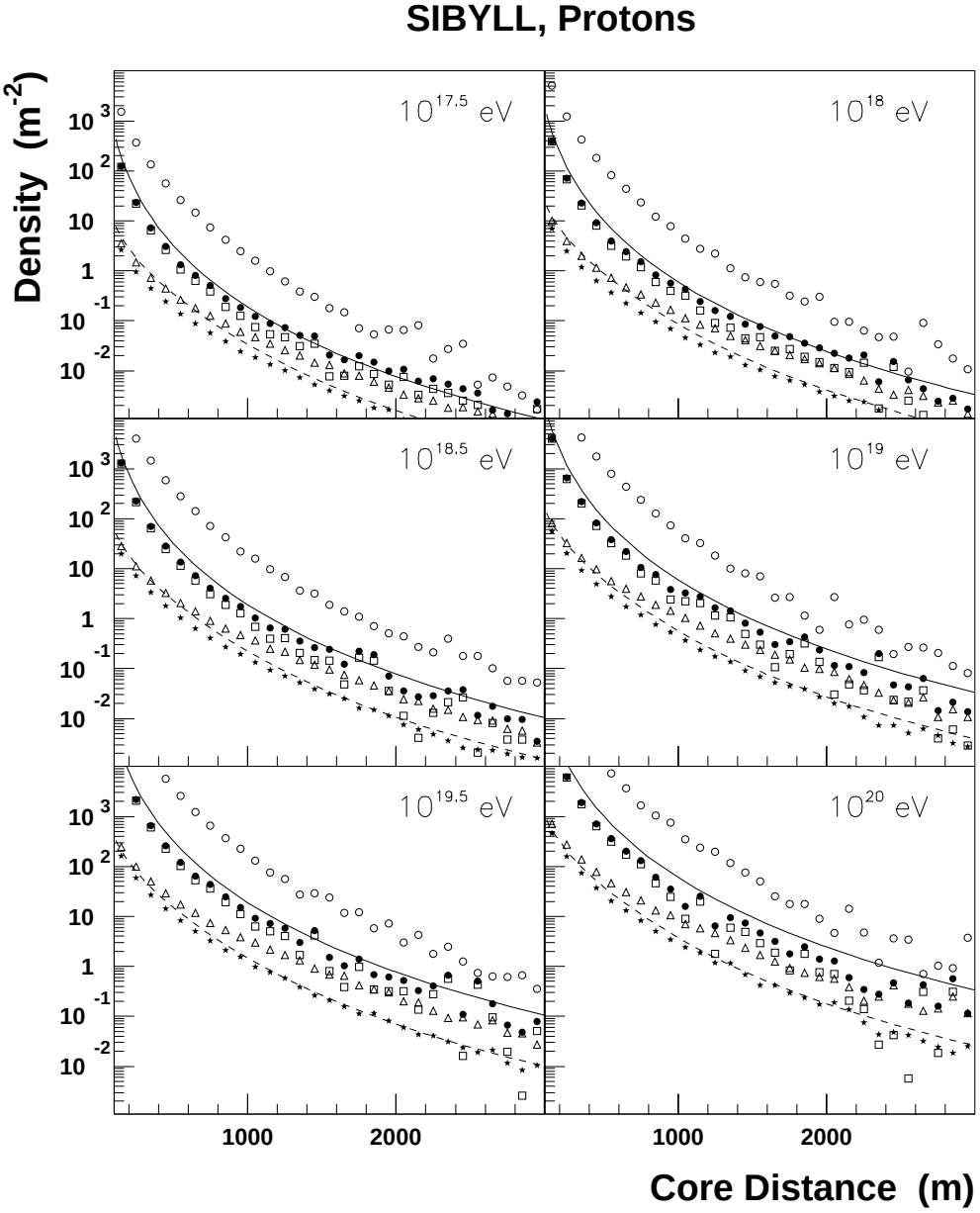

Figure 6: *Same as Fig. 5 except for the SIBYLL hadronic interaction model being used.*

0.05 MeV), the change of the *form*[3] of the lateral distribution of charged particles

[3]The densities may be shifted vertically to compare the form of the lateral distribution with the experimental points, since the primary energy in the experiment is given by the conversion equation by Dai et al.

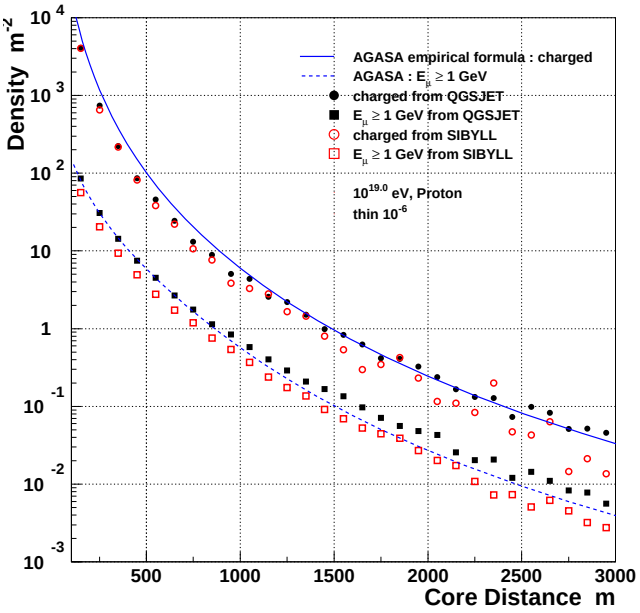

Figure 7: *The lateral distributions of charged particles and muons above 1 GeV simulated with the QGSJET model and the SIBYLL model are compared for proton primary. The thinning level is 10^{-6} and the cutoff energies of muons and electrons are 10 MeV and 1.0 MeV, respectively.*

is not significant. Therefore the cutoff energy of 1.0 MeV is used in the following simulations to save simulation time and storage of individual particle information.
Generally speaking, the agreement of the experimental lateral distributions of charged particles on surface and muons under absorber with the simulated distributions is quite well. The slight difference is observed within 1000 m from the core in case of charged particles and beyond 1000 m in case of muons above 1 GeV. The former is related to the assignment of the primary energy and will be discussed in Section 5.

4.2.1 Energy dependence

In Fig. 5, the primary energy dependence of the lateral distributions of each component is shown for proton primaries with the QGSJET model. Closed circles are the lateral distributions of charged particles (muons and electrons) and the solid and dashed lines represent the empirical formula of the AGASA experiment. Considering the difference of the primary energy assignment in the experiment and the simulation, if we shift the simulated points upward to fit the experimental ones within 1000 m from the core, the shapes are in good agreement with experimental results up to 1000 $\sim$ 2000 m from the core.
The energy *independence* of the lateral distribution of charged particles at the surface

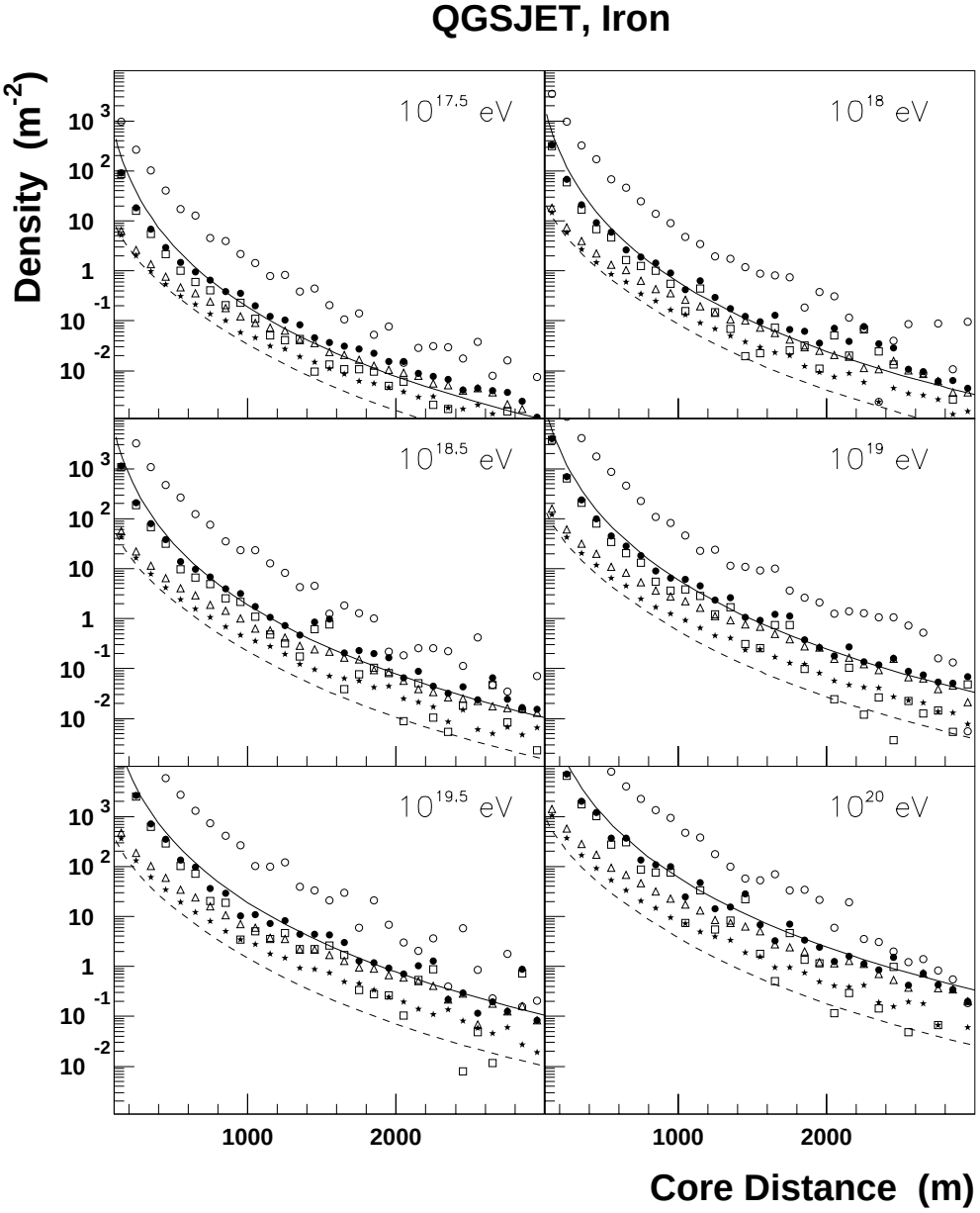

Figure 8: *Same as Fig. 5, except for the primary particle being iron.*

between $10^{17.5}$ eV and 10^{20} eV observed by the AGASA is well supported by the QGSJET model.

4.2.2 Hadronic model dependence

The lateral distributions of charged particles from SIBYLL are shown in Fig. 6. If we shift the simulated values upward, the expected lateral distributions are also fitted to the experiment, however, the deviation from experiment slightly increases as energy increases (Fig. 6).
Lateral distributions of charged particles and muons above 1 GeV in proton showers from QGSJET and SIBYLL models are compared in Fig. 7 for energy 10^{19} eV. While there is no big difference in charged particles for QGSJET and SIBYLL calculations, SIBYLL underestimates muons systematically by about a factor 1.6 with respect to QGSJET, and this would lead to a different interpretation of the experimental showers concerning their mass composition.
The absolute values are related to the assignment of the primary energy and will be discussed in Section 5.

4.2.3 Primary composition dependence

In Fig. 8, the lateral distributions of charged particles from iron primary are shown for six different primary energies. Energy *independence* of the form of the lateral distribution on primary energy is also accepted for the iron primary. Therefore the energy *independence* of lateral distribution of AGASA experiment can be understood irrespective of primary composition.
In Fig. 9, the lateral distributions of charged particles and muons above 1 GeV from proton and iron primaries are compared with the experiment. The difference of charged particle densities between proton and iron primaries is about 10 % around 600 m from the core and those of muons above 1 GeV is about 50 %.

4.3 Muon lateral distributions with different cutoff energies

In Figs. 10 and 11, lateral distributions of muons above 10 MeV, 0.25 GeV, 0.5 GeV, 1 GeV and 2 GeV are compared with the experimental formula of threshold energy of 1 GeV (Eq. (6)) at 10^{18} eV (left) and 10^{19} eV (right). The lateral distibutions become steeper as the cutoff energy increases. While for QGSJET calculations proton induced showers describe the experimental curve best, for SIBYLL simulations iron induced showers are closer to the experimental distributions.
It should be noted that the smaller muon number of SIBYLL model relative to other interaction models used in CORSIKA has been pointed out in the $10^{14} \sim 10^{15}$ eV region by Knapp et al.[23].

4.3.1 Primary energy dependence of ρ_μ(600)

The energy spectra of muons between 0.25 GeV and 1.5 GeV at 600 m from the core [30] are compared with the simulation results by the QGSJET and the SIBYLL models, and proton and iron primaries for 10^{19} eV showers in Fig. 12. The slope of

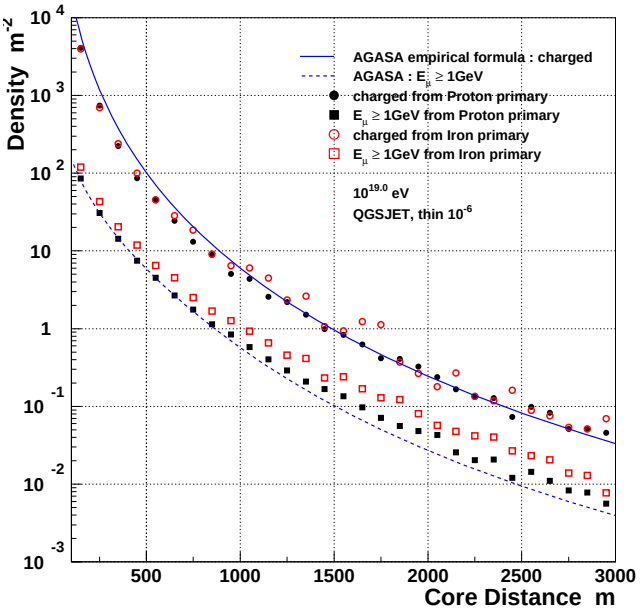

Figure 9: *The lateral distributions of charged particles and muons above 1 GeV simulated with the QGSJET model for proton and iron primaries. The thinning level is 10^{-6} and cutoff energies of muons and electrons are 10 MeV and 1.0 MeV, respectively.*

the spectrum increases with core distance, but does not depend on composition. The muon densities from proton primary with the QGSJET model are similar to those from iron primary with the SIBYLL model. The slope of experimental results agrees well with the simulated ones except at 0.25 GeV, where we have in the experiment punch-through of the electromagnetic component into the muon detectors, even at 600 m from the core.

The ratio of the muon densities above 0.5 GeV and 1.0 GeV is plotted in Fig. 13 as a function of core distance. The ratio at 600 m from the core coincides with experiment, however, it increases with core distance. The ratio does not depend on primary energy.

The relation of muon density above 1 GeV at 600 m from the core ($\rho_\mu(600)$) with the primary energy for three different conditions is compared in Fig. 14. The slope α in $\rho_\mu \propto E^\alpha$ and the density at 10^{19} eV are compared in Table 1. The results by the SIBYLL model with the MOCCA code [16] are also listed for comparison. Though the hadronic model is the same, there is about 10 % difference in density between the results based on the two different simulation codes. The box indicated in Fig. 14 by a solid line is the experimental relation derived by AGASA. The slopes from simulation are steeper than that from the experiment. Here the energy in the experimental results is assigned by Eq. (1). This result is claimed by Dawson et

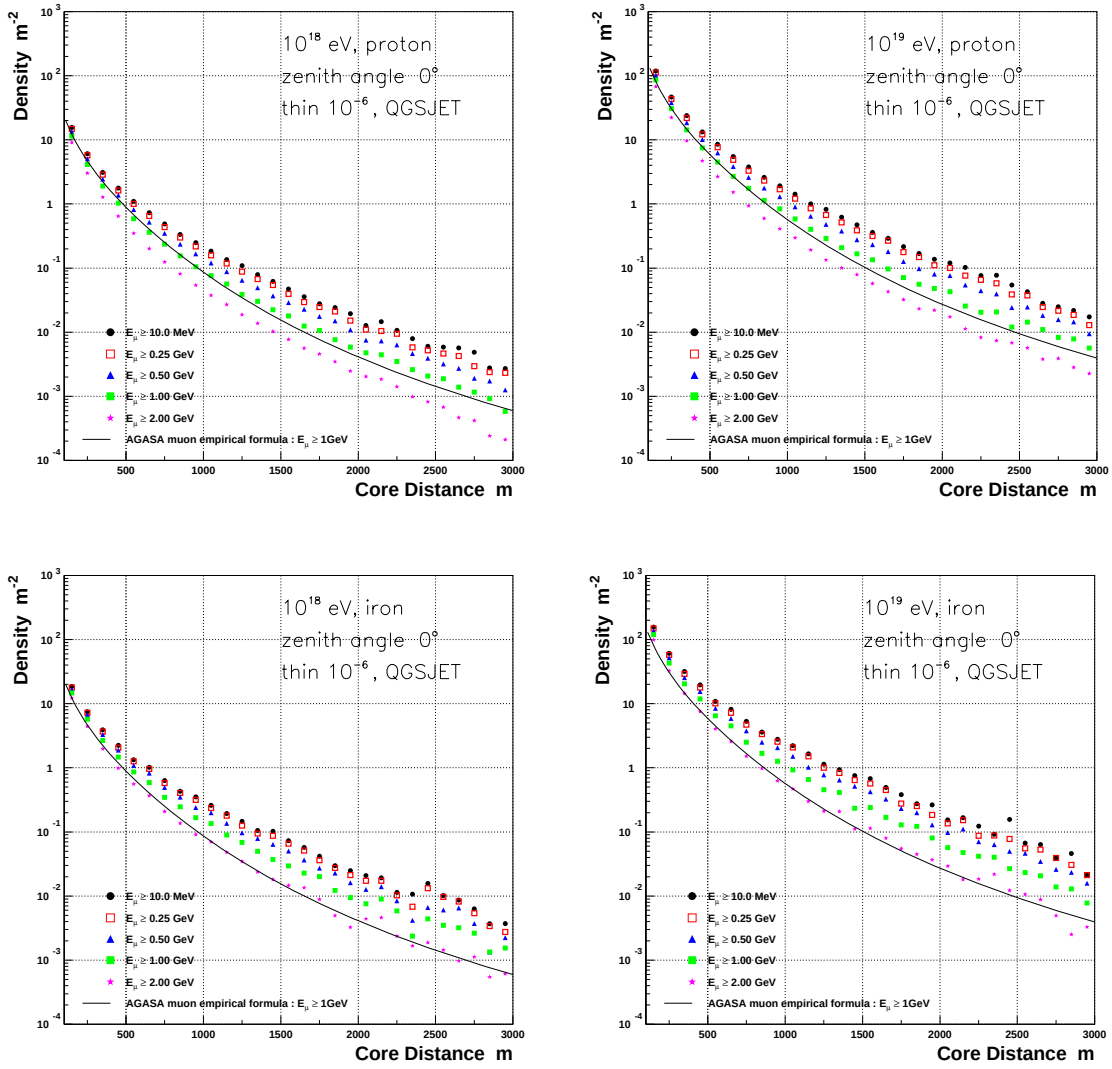

Figure 10: *The lateral distributions of muons of cutoff energies above 10 MeV, 0.25 GeV, 0.5 GeV, 1.0 GeV and 2.0 GeV. QGSJET model. The thinning level is* 10^{-6}. *Upper figures are proton primaries and lower ones are iron. The incident energies are* 10^{18} *eV (left) and* 10^{19} *eV (right), respectively.*

al. [16] as a supporting evidence that the composition changes from predominantly heavy around $10^{17.5}$ eV to predominatly light around $10^{19.0}$ eV. This will be discussed in Section 5.

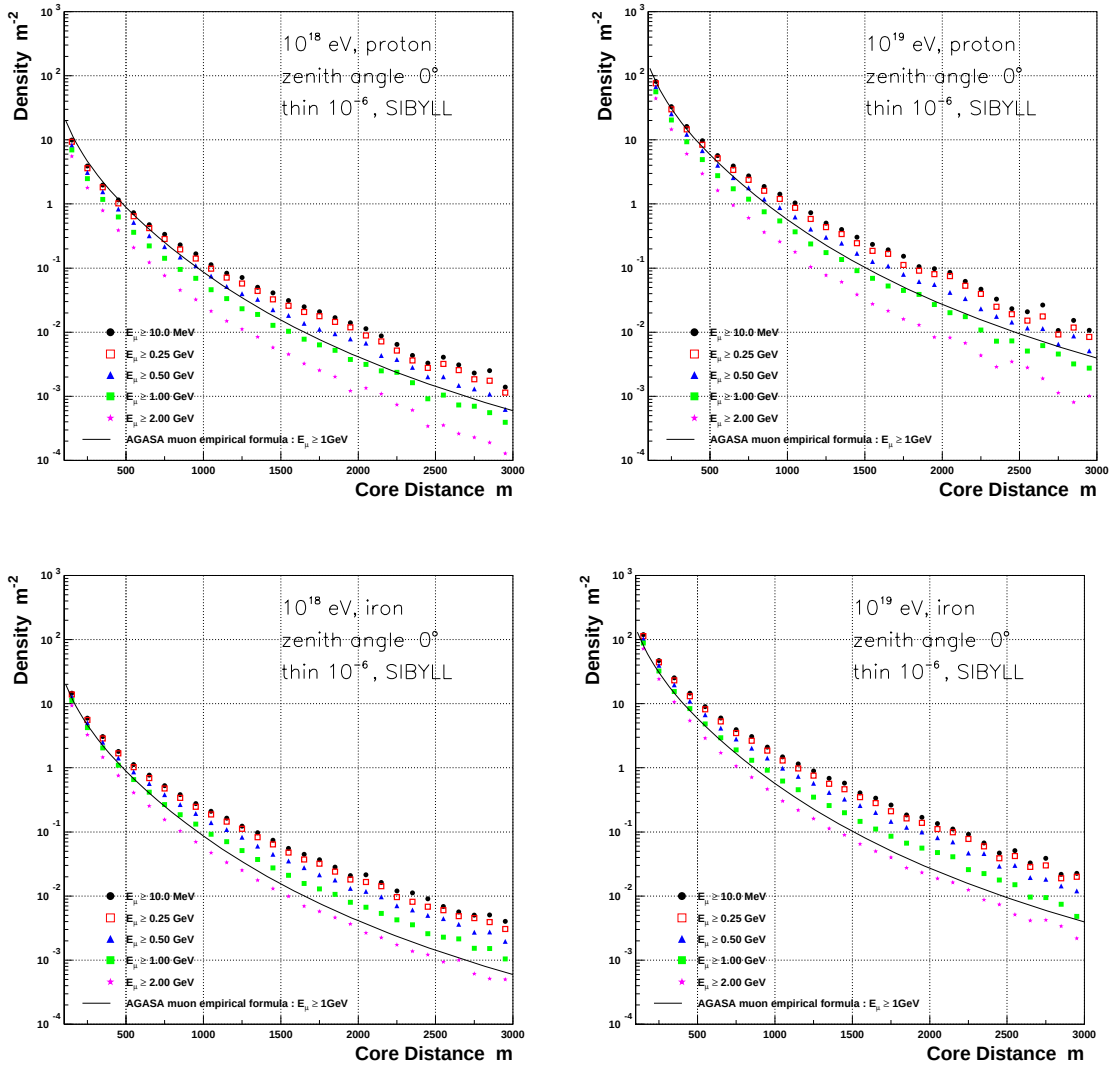

Figure 11: *Same as Fig. 10, except for the hadronic interaction model is being SIBYLL.*

4.4 Charged particle densisy, S(600)

4.4.1 Energy dependence

In Fig. 15, the relation of S(600) with the primary energy is plotted for various conditions. The solid line is the relation used by AGASA (Dai et al. [6]).
S(600) does not depend on interaction model (QGSJET, SIBYLL) nor primary mass (proton, iron) within 20 % which supports the previous simulations by Hillas [5] and Dai et al. [6]. The S(600) vs. primary energy relation is almost linear irrespective of primary mass (proton or iron) in case of QGSJET, however, S(600) $\sim$ $E^{0.97}$ in case of SIBYLL (Fig. 15).

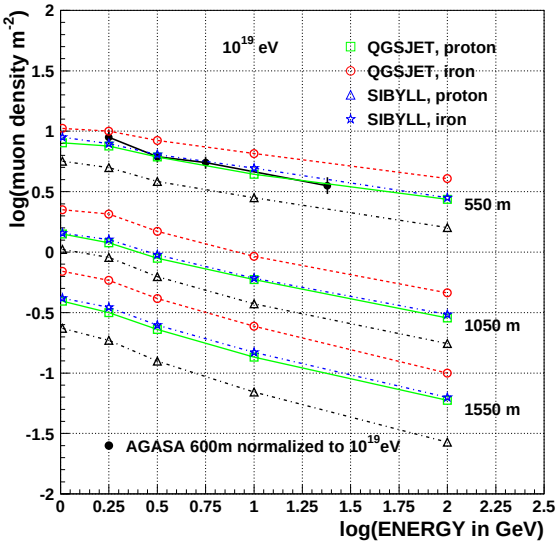

Figure 12: *Energy spectra of low energy muons at core distance 550 m, 1050 m and 1550 m are drawn for 10^{19} eV proton and iron primaries and QGSJET and SIBYLL models. Experimental results of Akeno experiment at 600 m from the core are plotted by normalizing primary energy to 10^{19} eV.*

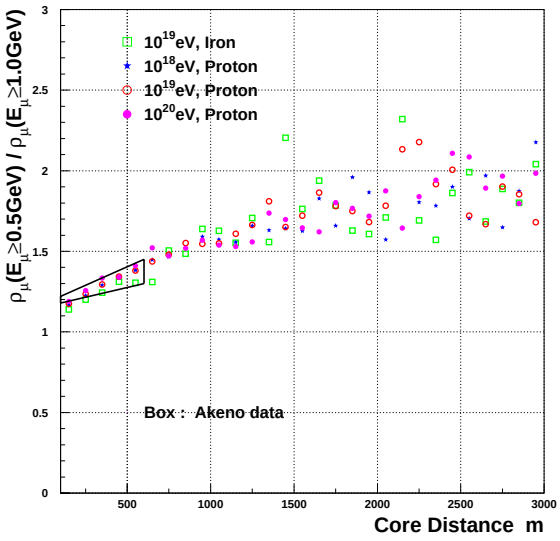

Figure 13: *Ratio of muon densities $\rho_\mu(E_\mu > 0.5$ GeV$)/\rho_\mu(E_\mu > 1.0$ GeV$)$ as a function of core distance. QGSJET model. Experimental ratio of $\rho_\mu(E_\mu > 0.75$ GeV$)/\rho_\mu(E_\mu > 1.35$ GeV$)$ of Akeno experiment is shown as a box from 100 m to 600 m.*

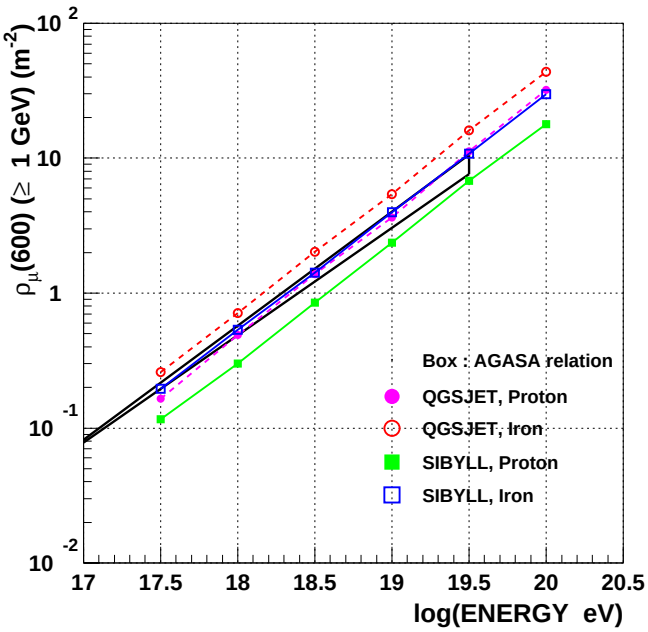

Figure 14: *Relation of $\rho_\mu(600)$ above 1 GeV with energy for various conditions. The boxes gives a result determined at Akeno.*

Table 1: *Comparison of slope and density at 10^{19} eV.*

code	model	primary	slope	$\rho_\mu(600)$ at 10^{19} eV	note
CORSIKA	QGSJET	proton	0.92	3.85	
CORSIKA	QGSJET	iron	0.89	5.64	
CORSIKA	SIBYLL	proton	0.88	2.39	
CORSIKA	SIBYLL	iron	0.87	3.96	
MOCCA	SIBYLL	proton	0.90	2.95	[29]
MOCCA	SIBYLL	iron	0.86	4.57	[29]

There are clear differences between the simulated number of charged particles and the relation used at AGASA, though the number of charged particles depends on the cutoff energy of electrons. The details will be discussed in Section 5.

4.4.2 Fluctuations

It is quite important to know how much S(600) fluctuates shower by shower in order to compare with the experimental observables quantitatively. We have not yet simulated enough number of showers to study fluctuations. In the following we show some

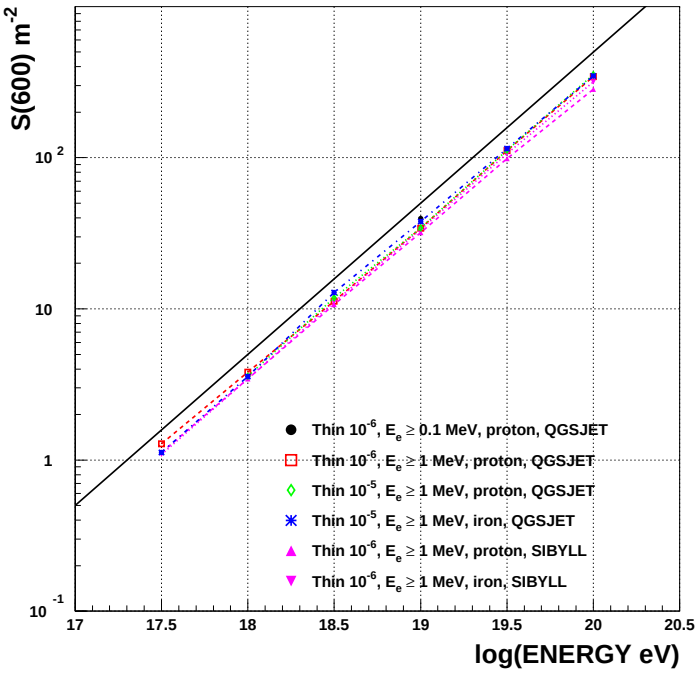

Figure 15: *Relation of charged particle density at 600 m from the core (S(600)). The solid line is the relation used by AGASA (Dai et al.).*

examples. In Fig. 16 lateral distributions of photons, electrons and muons for 10 showers for proton primary of $10^{19.0}$ eV are shown.
In Fig. 17, relative fluctuations around the average densities of photons, electrons, charged particles, muons above 10 MeV and 1 GeV are shown as a function of core distance for proton (left) and iron (right) primaries of 10^{19} eV. 30 showers are used in each figure. In case of proton showers, the fluctuation decreases as core distance increases up to about 500 m, while it is almost constant in case of iron primary. The increase of fluctuations beyond several hundred m is partly due to the statistics of the simulated particles and the fluctuations decrease as the thinning level decreases. Though a thinning level of $10^{-6.5}$ is used, the statistics is still not enough beyond more than several hundred m from the core.

4.5 Zenith angle dependence of charged particles

There is a zenith angle dependence in the lateral distribution of charged particles in the AGASA experiment and the slope parameter η is expressed by Eq. (5) as a function of zenith angle.
In Fig. 18, the lateral disribution of charged particles at a zenith angle of 40° is shown for proton primaries of six primary energies. For the AGASA lateral distribution, $\eta = 3.6$ and an attenuation length $= 500 gcm^{-2}$ are used. It is shown that the

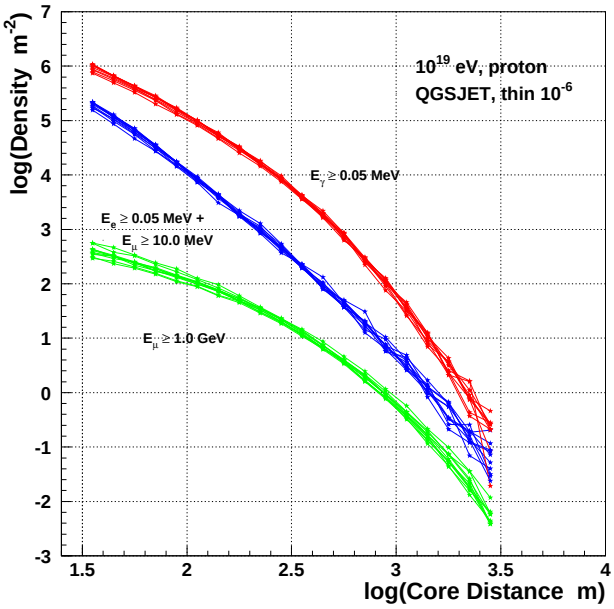

Figure 16: *Fluctuation of lateral distributions of 10 showers.*

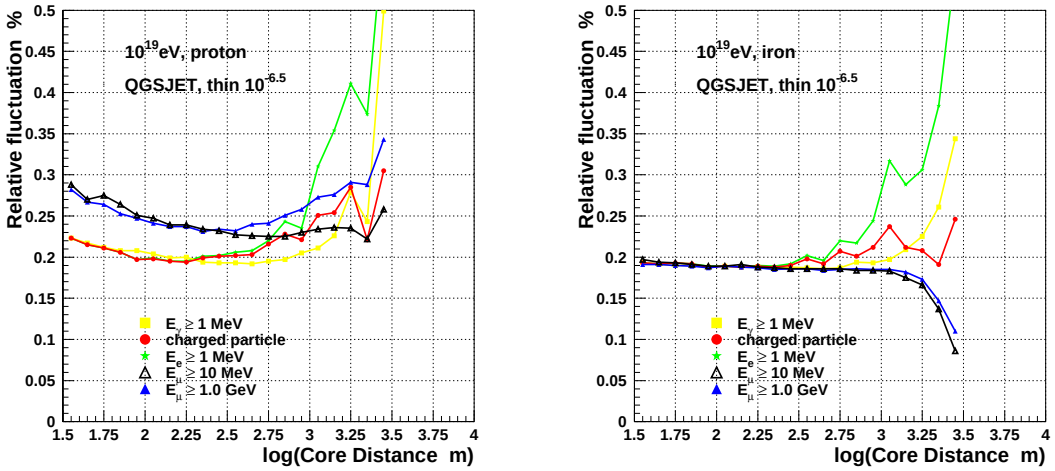

Figure 17: *Relative fluctuations around the average densities of photons, electrons, charged particles, muons above 10 MeV and 1 GeV as a function of core distance. Proton (left) and iron (right) primaries of 10^{19} eV. QGSJET and the thinning level of $10^{-6.5}$. 30 showers are used in each figure.*

simulated results fit well to the experimental function including the absolute values, independent of primary energy.

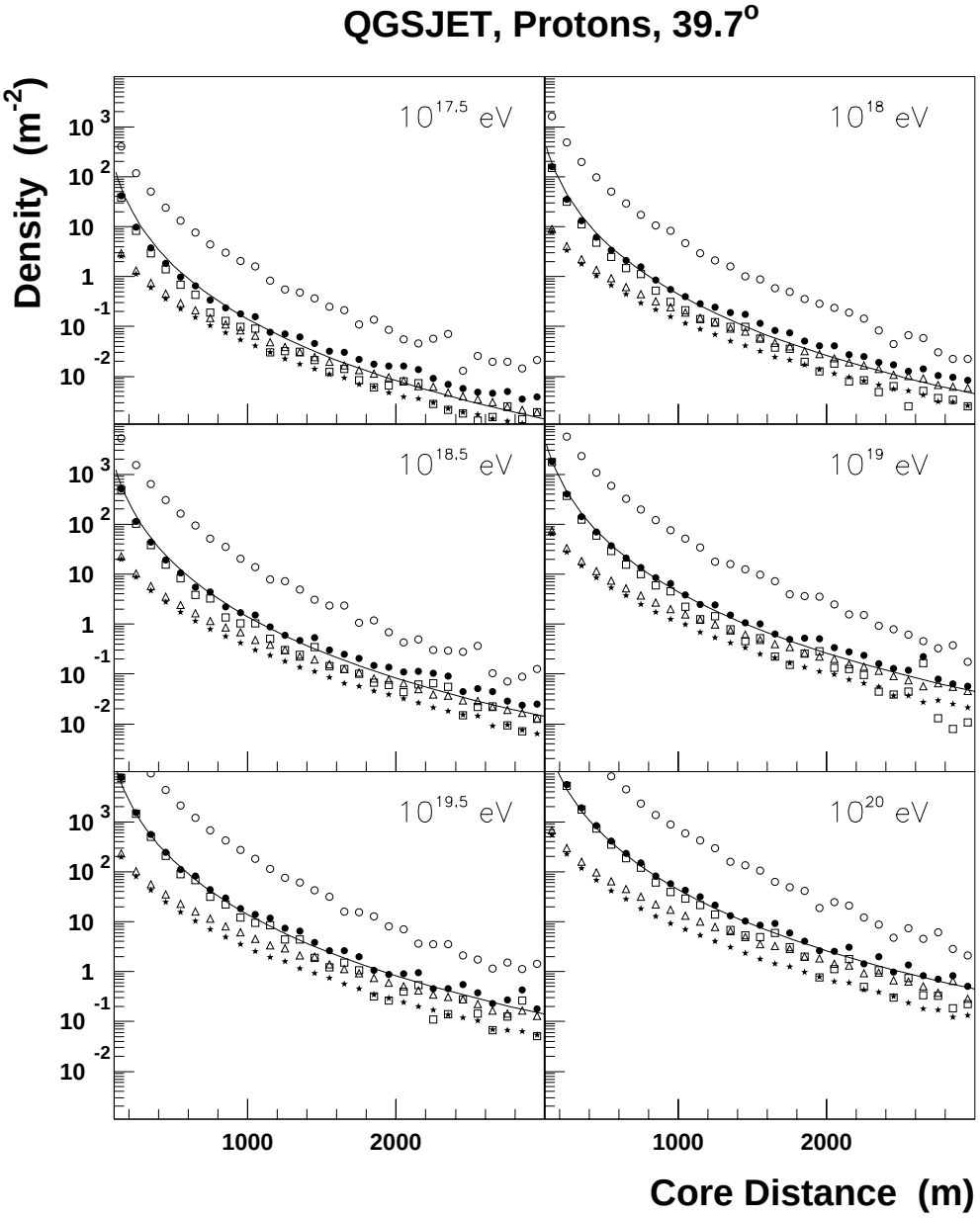

Figure 18: *The lateral distributions of photons, electrons, muons and charged particles simulated at a zenith angle of 39.7°. The thinning level is 10^{-6} and the cutoff energy of muons is 10 MeV and those of electrons and photons are 1.0 MeV. For drawing the AGASA lateral distribution, an attenuation length of 500 g cm^{-2} is used and the change of η with zenith angle is taken into account.*

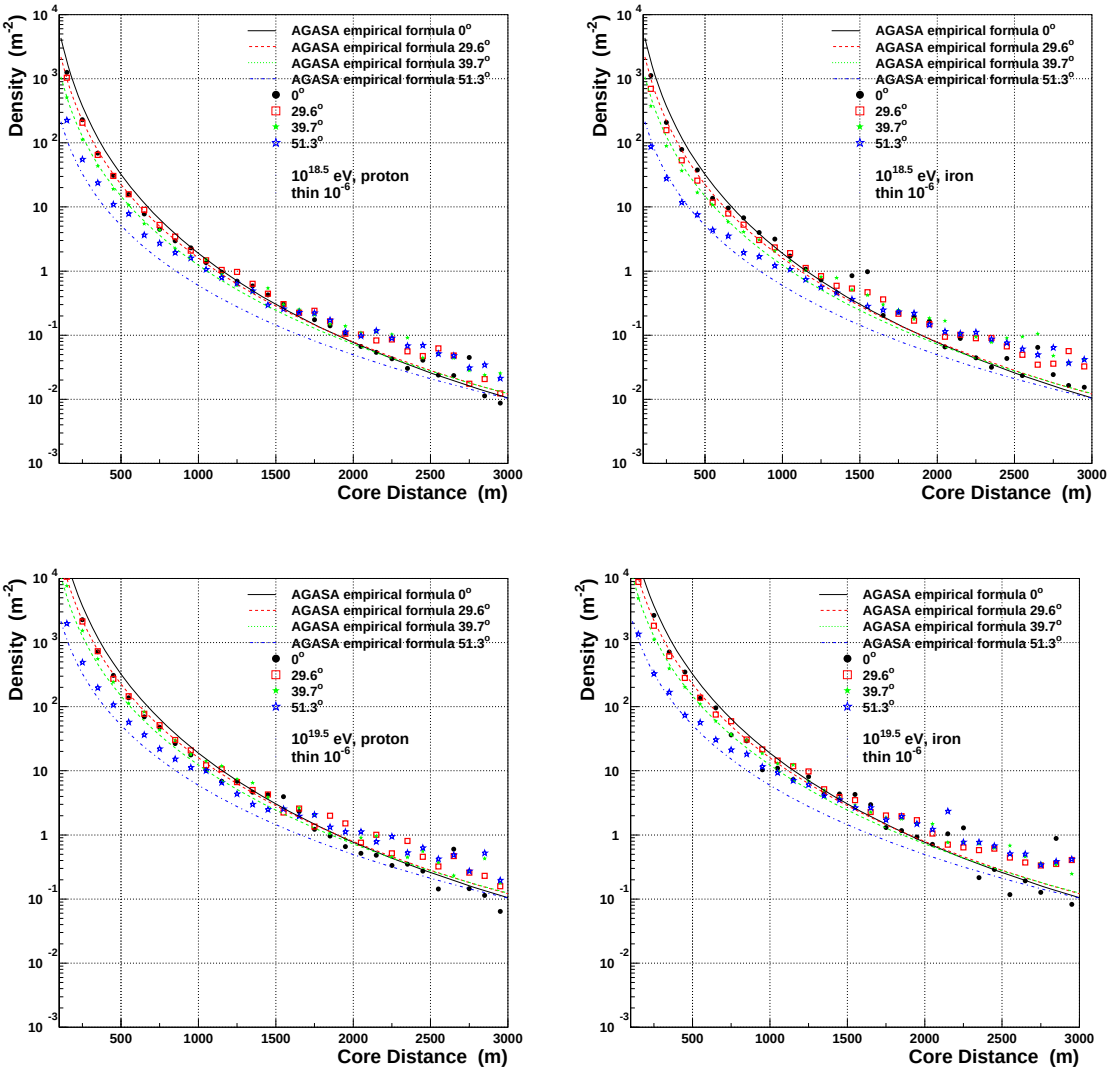

Figure 19: *The lateral distributions of charged particles at four zenith angles 0°, 29.6°, 39.7°, and 51.3° for primary energies $10^{18.5}$ eV (top) and $10^{19.5}$ eV (bottom). QGSJET model and cutoff energy of muons is 10 MeV and those of photons and electrons are 1.0 MeV. The left figure is for proton primary and the right one is for iron primary.*

Fig. 19 shows the lateral distributions of charged particles at the four zenith angles 0°, 29.6°, 39.7° and 51.3° for proton (left) and for iron (right) primaries and for primary energies $10^{18.5}$ eV and $10^{19.5}$ eV, respectively.
The $S_\theta(600)$ values obtained are plotted in Fig. 20 as a function of atmospheric depth ($sec\ \theta$) and connected with lines. The solid lines represent proton primaries and dotted ones are iron primaries. It should be noted that there are no differences in attenuation of charged particles with zenith angle between proton and iron primaries.

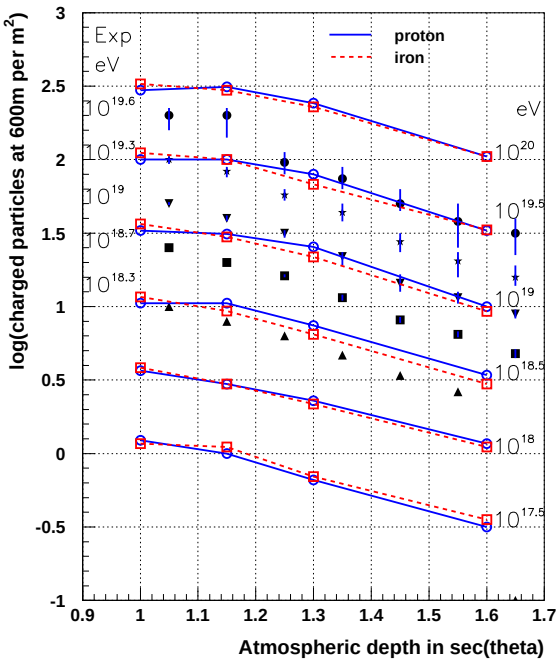

Figure 20: *The variation of S(600) with zenith angle shown in Fig. 2 is compared with the zenith angle dependence of charged particles at 600 m ($\rho_{ch}(600)$) (electrons $\geq$ 1 MeV and muons $\geq$ 10 MeV) determined by CORSIKA. The closed symbols are experimental points, corresponding to energies $10^{19.6}$ eV, $10^{19.3}$ eV, $10^{19.0}$ eV, $10^{18.7}$ eV and $10^{18.3}$ eV from top to bottom. Open circles and squares are from CORSIKA (QGSJET model, thinning level 10^{-6} and cutoff energy of muons is 10 MeV and those of photons and electrons are 1.0 MeV). Solid lines are from proton and dotted are from iron primaries.*

The experimental points are obtained using the method of 'equi-intensity cuts' on the integral $S_\theta(600)$ spectra, based on the assumption that the flux of showers above a certain primary energy does not change with atmospheric depth [20]. The experimental points especially for neally vertical showers can be fitted neither by proton primary, nor by iron primary. This point will be discussed in Section 5.

5 Discussion

The general features of the electromagnetic component and the low energy muons observed by AGASA can be well reproduced by CORSIKA simulation, except the slight differences in the abolute values. These discrepancies in abolute values between experiment and simulation results are partly due to the assignment of primary energy,

which depends on the definition of a single particle used in experiment and simulation. More remarkable discrepancies are the slope of ρ_μ vs. S(600) relation and zenith angle dependence $S_\theta(600)$ for constant primary energy.
In the following we evaluate the simulated results with a similar definition of each observable in AGASA experiment.

5.1 Definition of density used in Akeno/AGASA experiment

In the AGASA experiment, a scintillator of 5 cm thickness is used to detect particles on the surface. The scintillator is placed inside an enclosure made of iron of 1.5 $\sim$ 2 mm thickness and the detector is in a hut whose roof is made of an iron plate of 0.4 mm thickness.
The definition of a single particle at Akeno experiment (V_1) is the *average* of the pulse-height distribution of muons traversing vertically a scintillator [9]. V_1 is 10 % larger than the peak value, since the distribution is not Gaussian, but subject to Landau fluctuation. If we use a peak value in pulse *height* distribution (PHD) of omnidirectional particles, the peak value V_{ph} is accidentally coincident with V_1 at Akeno level ($V_{ph} \simeq V_1$). In order to convert a density measured by scintillator to an electron density corresponding to the calculated density by the NKG function, the density measured by scintillators and spark chambers at the Institute for Nuclear Study at Tokyo [40] is used at Akeno. This ratio is 1.1 between 10 m and 100 m from the core and hence the electron shower size (N_e) determined by the Akeno 1 km^2 array was reduced by 10 % from the calculated N_e [9].

In AGASA a peak value V_{pw} in the pulse *width* distribution (PWD) of omnidirectional muons on a 5 cm scintillator is used as a single particle conventionally. The pulse width is obtained by discriminating a signal, which decays exponentially with a time constant of 10 μsec, at a constant level. V_{pw} is not equal to V_{ph} and is related to V_{ph} as :

$$V_{pw} = (V_{ph} + \sqrt{V_{ph}^2 + \sigma^2})/2$$

where σ is a full width at half maximum in PHD [35]. By putting V_{ph}=1.0 and σ=0.70, V_{pw}=1.1. A conventional value, V_{pw}, used at AGASA corresponds to $1.1 \times V_1 (\simeq 1.1 \times V_{ph})$. That is V_{pw} corresponds to a measured density by spark chamber or the electron density, as far as the ratio of the density measured by scintillators and the spark chambers is 1.1.

Though there is a transition effect of the electromagnetic component in scintillator of 5 cm thickness within 30 m from the core [9], the density of charged particles as expressed in units of V_1 does not depend on the thickness of the scintillator above 30 m from the core as shown experimentally in Teshima et al. [36]. This can be understood since the radiation lengths of scintillator and air are very similar, so that the fraction of electrons at any depth in the scintillator changes only slowly as

compared to air. This independence of thickness of scintillator is also shown by a simulation by Cronin [14] and Kutter [15].
Assuming the 10 % difference of scintillator density to spark chamber density at 600 m from the core, the density in units of V_{pw} ($1.1 \times V_{ph}$) coincide with spark chamber density as described above and Eq. (1) was applied to deriving the AGASA energy spectrum.

5.2 Densities measured by scintillator of 5 cm thickness

So far the AGASA group has used a factor 1.1 of scintillator density to spark chamber density which is determined within 100m from the core [40], however, the factor has not been yet measured beyond 100 m from the core. In the following we discuss the lateral distribution of energy losses by photons, electrons and muons in 5 cm scintillator in units of V_{pw} at Akeno level, taking into account the incident angles of electrons and photons far from the core, because the incident angles of electrons and photons on scintillator may not be vertical even for a vertical shower and the particles have some angular distribution.
In Fig. 21 the energy spectra of photons, electrons and muons are shown at core distances between 500 m and 800 m, simulated by CORSIKA. There remain still many photons at a zenith angle of 51.3° ($sec\ \theta = 1.6$).
In CORSIKA, in a shower the incident angle of each particle to the surface is recorded, so that we can calculate the energy loss of each particle which is incident on the scintillator with various zenith angles. In case of electrons and muons, only ionization

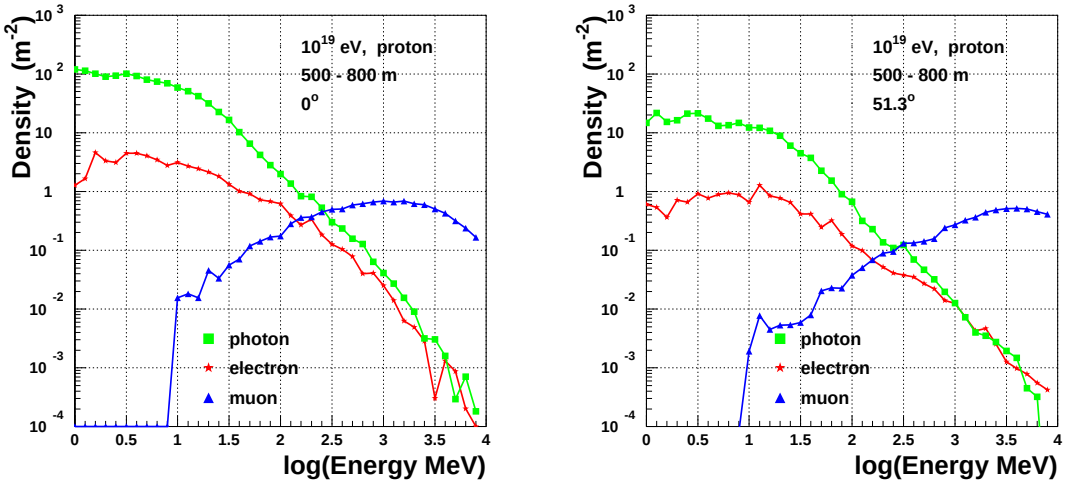

Figure 21: *Energy spectra of photons, electrons and muons at core distance between 500 m and 800 m. The primary particle is a proton of 10^{19} eV. Zenith angles are 0° (left) and 51° (right).*

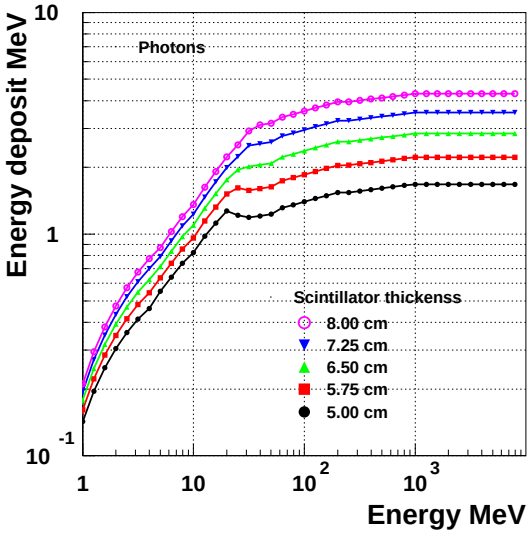

Figure 22: *Average energy loss of a photon in scintillators of various thicknesses.*

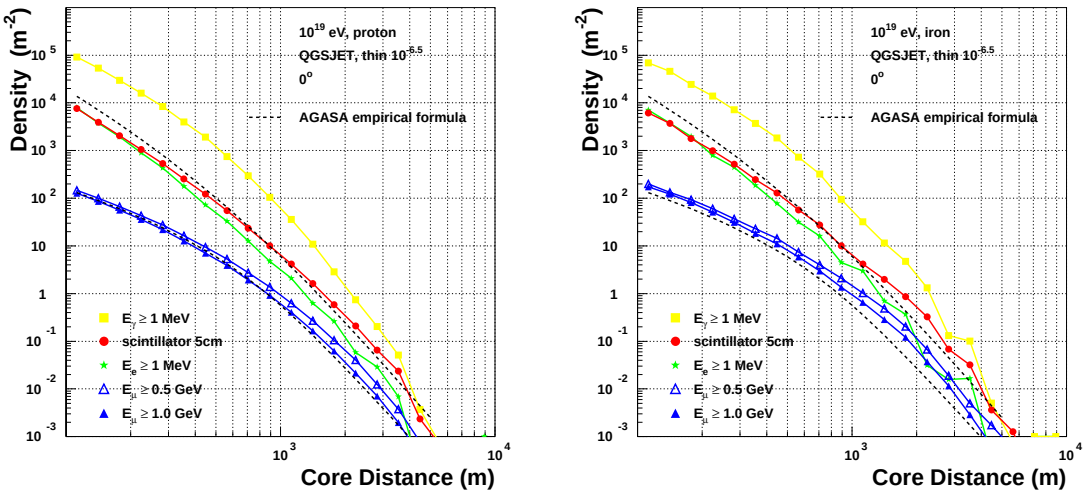

Figure 23: *Lateral distribution of energy deposit in scintillator (•) of 5 cm thickness (ρ_{sc}) in units of V_{pw} is compared with the experimental lateral distribution of AGASA. Those of electrons ($\geq$ 1 MeV), photons ($\geq$ 1 MeV), muons ($\geq$ 0.5 GeV) and muons ($\geq$ 1 GeV) are also shown. The upper figure is proton primary and the lower one iron.*

loss is taken into account. The energy loss of photons is evaluated as follows. By dividing the scintillator in thin layers, the fraction of conversion to electrons in each layer is calculated by using the photon attenuation length in water [38]. The energy

loss of electron or electron/positron in the remaining layers for the fraction of photons is calculated. The average energy loss of a single photon in a scintillator of various thicknesses is shown in Fig. 22 as a function of the photon energy. Though the calculation process is simple, the result for a scintillator of 5 cm thickness agrees well with the Monte Carlo simulation results by Kutter [15].
The density of a shower of zenith angle θ is evaluated as the energy loss in scintillator of $5 \times sec\ \theta$ cm thickness (in units of V_{pw}) in an area of $1 \times \cos\theta$ m^2.

In Fig. 23, the lateral distribution of energy deposit in scintillator of 5 cm thickness in units of V_{pw} (ρ_{sc}) is plotted and compared with that of the experimental lateral distribution (dashed line). The simulated lateral distribution is flatter than the experimental one. ρ_{sc} reflects the number of electrons near the core (up to about 200 m from the core), but becomes larger than the electron density with core distance. Though the agreement of $\rho_{sc}(600)$ with the experimental S(600) is quite good, the difference of the lateral distribution of ρ_{sc} from the experiment must be studied further.

5.3 Primary energy and S(600) relation evaluated by CORSIKA

In Table 2, the density of charged particles at 600 m from the core, $\rho_{ch}(600)$, or the scintillator density of 5 cm thickness, $\rho_{sc}(600)$, are listed for showers of 10^{19} eV of vertical incidence.
The various combinations of simulation codes (CORSIKA, MOCCA), hadronic interaction models (QGSJET, SIBYLL), primary species (proton, iron), thinning levels and threshold energies of electromagnetic components are compared.
In general, the difference of $\rho_{ch}(600)$ due to the difference of simulation codes or hadronic interaction models is within 10 % for the same cutoff energy of electromagnetic component.
$\rho_{ch}(600)$ depends on the cutoff energy of electromagnetic component. In the S(600) vs. energy relation by Dai et al. (Eq.(1)), the electromagnetic component with energy of less than the thinning level are connected to the NKG function without cutoff energy for electrons and photons, and MU at 2 radiation length above the observation level is used. The result by CORSIKA simulated with the similar method is given in the Table 2 as QGSJET-NKG. In case of CORSIKA, the relation is

$$E(eV) = 2.2 \times 10^{17} S(600)^{1.0} \tag{9}$$

and is about 10 % larger than that by Dai et al.
The energy losses of photons, electrons and muons in scintillator of 5 cm thickness ($\rho_{sc}(600)$ in units of V_{pw} have been evaluated as described in the previous section by taking into account their incident angle to the scintillator and attenuation of low energy photons and electrons in a scintillator container and hut.

Table 2: *Comparison of charged particle density (ρ_{ch}) or scintillator density in units of V_1 (ρ_{sc}) at 600 m from the core for showers of vertical incidence, 10^{19} eV and proton or iron primary.*

code	model	primary	thinning level	$E_{e\gamma}$ (MeV) threshold	$\rho_{ch}(600)$ or $\rho_{sc}(600)$ m^{-2}	note
CORSIKA	QGSJET	proton	10^{-5}	1	32.5	
CORSIKA	QGSJET	proton	10^{-6}	1	32.4	
CORSIKA	QGSJET	proton	10^{-6}	0.1	37.5	
CORSIKA	QGSJET	proton	10^{-6}	0.05	39.1	
CORSIKA	QGSJET	iron	10^{-5}	1	35.7	
CORSIKA	QGSJET	iron	10^{-5}	0.05	39.8	
CORSIKA	SIBYLL	proton	10^{-6}	1	30.4	
CORSIKA	SIBYLL	iron	10^{-6}	1	33.5	
CORSIKA	QGSJET	proton	10^{-6}	1	38.0	
	-NKG			0	45.0	
CORSIKA	QGSJET	proton	10^{-6}	1.0	sci. 43.0	
CORSIKA	QGSJET	iron	10^{-5}	1.0	sci. 46.2	
CORSIKA	SIBYLL	proton	10^{-6}	1.0	sci. 38.2	
CORSIKA	SIBYLL	iron	10^{-6}	1.0	sci. 44.4	
MOCCA	SIBYLL	proton		0.1	33.5	Cronin [1]
		iron		0.1	38.7	Cronin [1]
COSMOS	QCDjet	proton	10^{-5}	0	50.0	Dai et al.[2]
	-NKG	CNO	10^{-5}	0		
		iron	10^{-5}	0		

[1] Simulation results made at Fermi Lab. using the SIBYLL interaction model with MOCCA simulation code. (J. Cronin [14]) [2] Two dimensional simulation results made at ICRR by COSMOS by Dai et al. Photons and electrons of energies below the thinning energy level are connected to the NKG function in which the Molière length is used at 2 radiation lengths above the Akeno altitude.

The relation is drawn in Fig. 24 for proton and iron primary. For QGSJET hadronic interaction model,

$$E(eV) = 2.07 \times 10^{17} S(600)^{1.03} \quad for \;\; proton \tag{10}$$

$$E(eV) = 2.24 \times 10^{17} S(600)^{1.00} \quad for \;\; iron \tag{11}$$

and for SIBYLL,

$$E(eV) = 2.30 \times 10^{17} S(600)^{1.03} \quad for \;\; proton \tag{12}$$

$$E(eV) = 2.19 \times 10^{17} S(600)^{1.01} \quad for \;\; iron. \tag{13}$$

Though there is a difference between proton and iron showers or QGSJET and SIBYLL, any combination assigns a higher energy than that by Eq. (1). If we

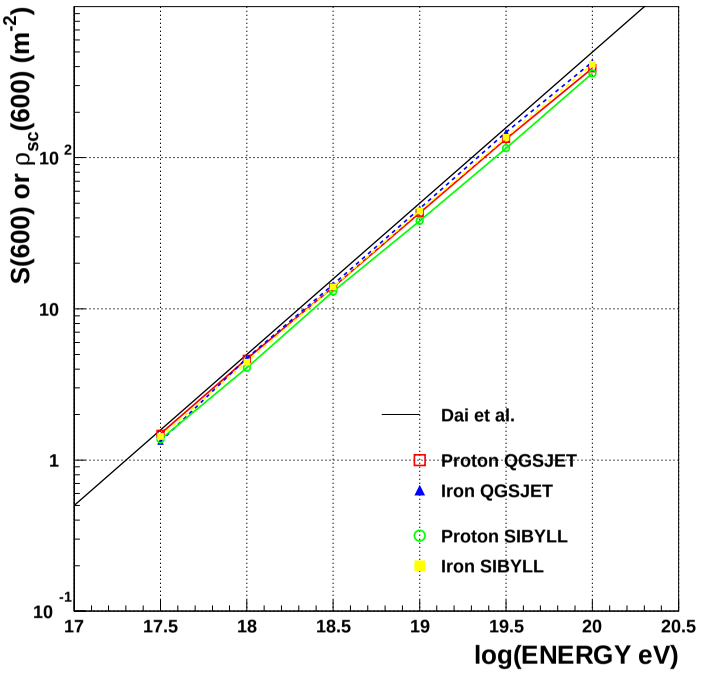

Figure 24: *S(600) or $\rho_{sc}(600)$ vs. energy relation estimated from the QGSJET and SIBYLL models for proton and iron primaries.*

apply the present stage of evaluation of the CORSIKA to the AGASA data, the following function from the average of Eq. (10) and Eq. (11) may be used as a conservative value.

$$E(eV) = (2.95 \pm 0.20) \times 10^{18} \left(\frac{S(600)}{14.25} \right)^{1.015 \pm 0.010} . \tag{14}$$

That means the energy of the AGASA events must be increased by 5 % at 10^{19} eV and 10 % at 10^{20} eV.

5.4 Composition from muon component

The slope of the $\rho_\mu(600)$ vs. energy relation is smaller in experiment than that in CORSIKA simulations. In Fig. 25 the $\rho_\mu(600)$ vs. S(600) (or $\rho_{sc}(600)$) relation is shown. The parameters of A and b in the following equation are listed in Table 3.

$$\rho_\mu(600) = A \times S(600)^b \tag{15}$$

The situation is not much different from the previous $\rho_\mu(600)$ vs. energy relation (Fig. 14), since the relation S(600) vs. energy is almost linear irrespective of primary composition or interaction model used.

Table 3: *Parameters of ρ_μ vs S(600) relation.*

Model	primary	A	b
QGSJET	proton	0.113	0.94
QGSJET	iron	0.189	0.89
SIBYLL	proton	0.085	0.91
SIBYLL	iron	0.141	0.88

.

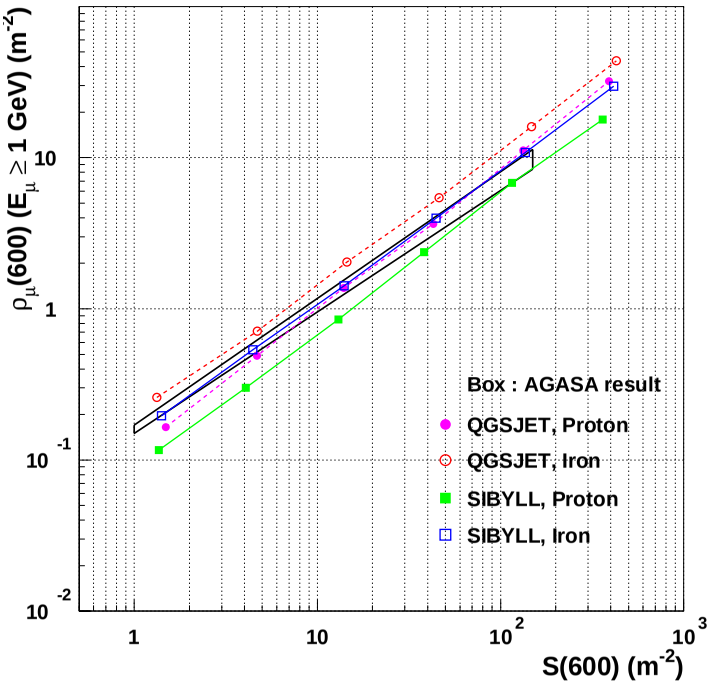

Figure 25: *ρ_μ vs. S(600) or ρ_{ch} relation from CORSIKA simulation.*

In order to explain this difference Dawson et al. [16] favours a likely change in mass composition from heavy to light at energies above 10^{18} eV, as a supporting evidence of the change of mass compositon claimed by the Fly's Eye experiment [17].
The difficulty of their interpretation arises when the relation is applied to the energy region lower than 10^{17} eV [4]. The comparison of N_μ vs N_e relation of the Akeno result [28] is compared with the result of KASCADE [39] in Fig. 26. The empirical formula

[4]The AGASA group claims that no change of composition around $10^{17.5}$ eV is observed by their experiment [28] against the Fly's Eye experiment. Dawson et al. don't argue on this point (compare with Figs. 4 and 6 of their paper). According to their figure, fraction of iron component is 100 % below $10^{17.5}$ eV in the Fly's Eye experiment, while that is 80 % at $10^{17.5}$ eV and exceeds 100 % below $10^{17.0}$ eV in the AGASA experiment. There is still no agreement between the two experiments below $10^{17.5}$ eV, which is the point in dispute.

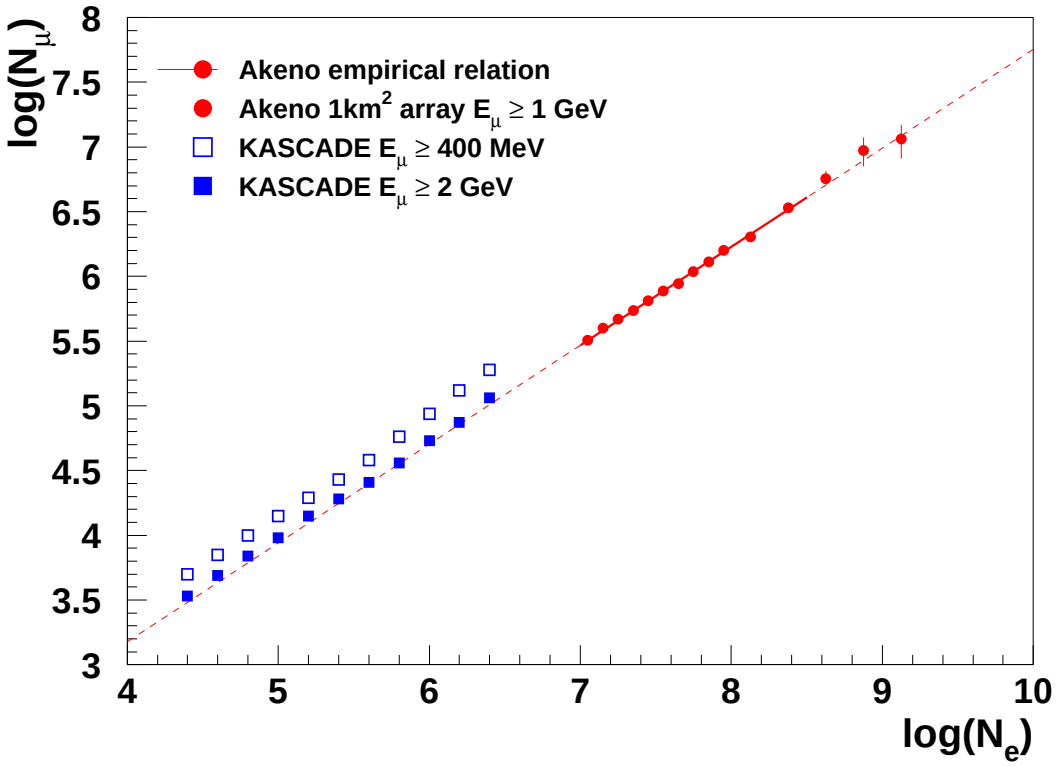

Figure 26: *N_μ vs. N_e relation of the Akeno and the KASCADE experiments. The solid line represents Eq. (16) and the dashed one is its extrapolation.*

of Akeno at $sec\ \theta = 1.05$ is expressed by

$$N_\mu = (2.94 \pm 0.14) \times 10^5 \times (N_e/10^7)^{0.76 \pm 0.02}. \tag{16}$$

Considering N_e attenuation from the Akeno level (920 g cm^{-2}) to the KASCADE level (1020 g cm^{-2}) and the difference of threshold energies of 1 GeV at the Akeno and 2 GeV at the KASCADE experiments, the agreement of extrapolation of the absolute values from both experiments are not accidental. The importance, however, is the agreement of the slopes of N_μ vs. N_e relation of both experiments in quite different energy regions.

Since in the higher energy region, N_e can not be determined by the AGASA, $\rho_\mu(600)$ vs. S(600) relation is evaluated. The result [28] is expressed as

$$\rho_\mu(600) = (0.16 \pm 0.01) \times S(600)^{0.82 \pm 0.03}, \tag{17}$$

which corresponds to the above equation in the overlapping energy region. Therefore the slope seems not to change from $10^{14.5}$ eV to 10^{19} eV. If we take the absolute values of SIBYLL model as used in Dawson et al. [16] (refer to Fig. 4 of their paper), the composition becomes heavier than iron below 10^{17} eV.

In drawing the line in Fig. 25, we have not taken into account the energy spectrum of the primary composition and the fluctuation around the average. Considering the

S(600) resolution in experiment becomes better as the energy increases, the difference of slopes in the experiment and the simulation may not be improved, even if we take into accout the fluctuation.
It should be noted that the difference of slopes between experiment and CORSIKA simulation may not be explained only by the change of composition with energy, since the difference of absolute values of muons between iron and proton primary is only a factor of $1.4 \sim 1.6$ ($0.15 \sim 0.20$ in log scale), while the difference of slopes is $0.07 \sim 0.09$.

5.5 Attenuation of S(600) with zenith angle and the implication on the primary composition around 10^{19} eV

As shown in Fig. 20, the variation of $\rho_{ch}(600)$ with zenith angle is very weak in CORSIKA as compared to the experiment. If we take into account the error in $\rho_{ch}(600)$ and zenith angle determination, this difference becomes larger. Since the experimental $\rho_{ch}(600)$ is increased by a factor of $e^{\sigma^2(\gamma-1)^2/2}$, where σ is the error in $\rho_{ch}(600)$ determination in a logarithmic scale and γ is the power index of the differential $\rho_{ch}(600)$ spectrum [41].

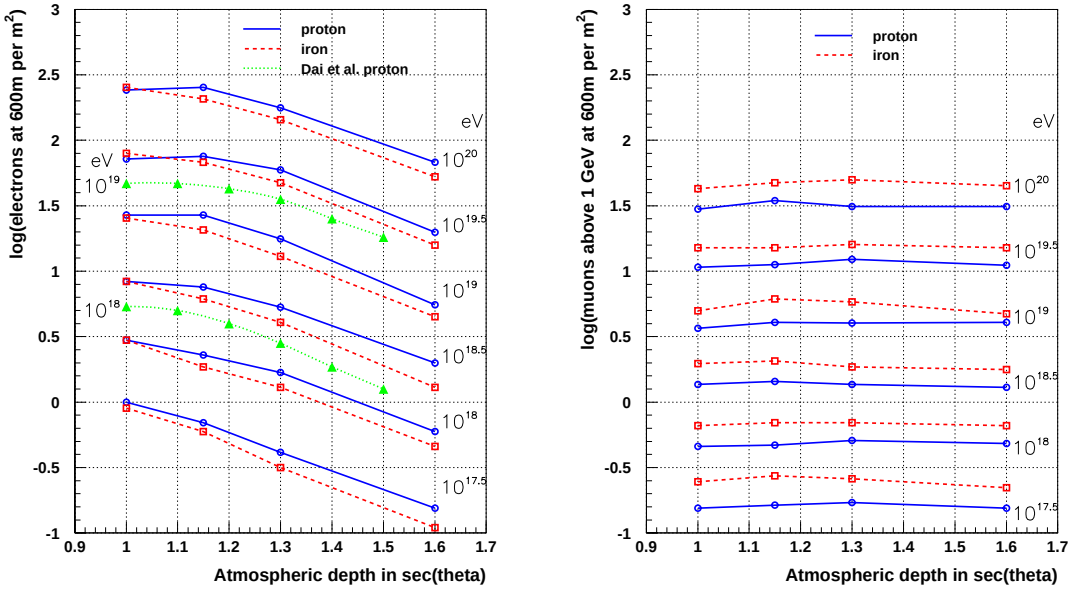

Figure 27: *The variation of electron density at 600 m from the core with zenith angle (left) and that of muon density above 1 GeV at 600 m from the core (right). Open symbols are from CORSIKA (QGSJET model, thinning level 10^{-6} and cutoff energy of electrons are 1.0 MeV). Solid lines are from proton primaries and dotted are from iron. Triangles connected with dotted lines are from Dai et al.[6] for primary protons of $10^{18.0}$ eV and $10^{19.0}$ eV, respectively.*

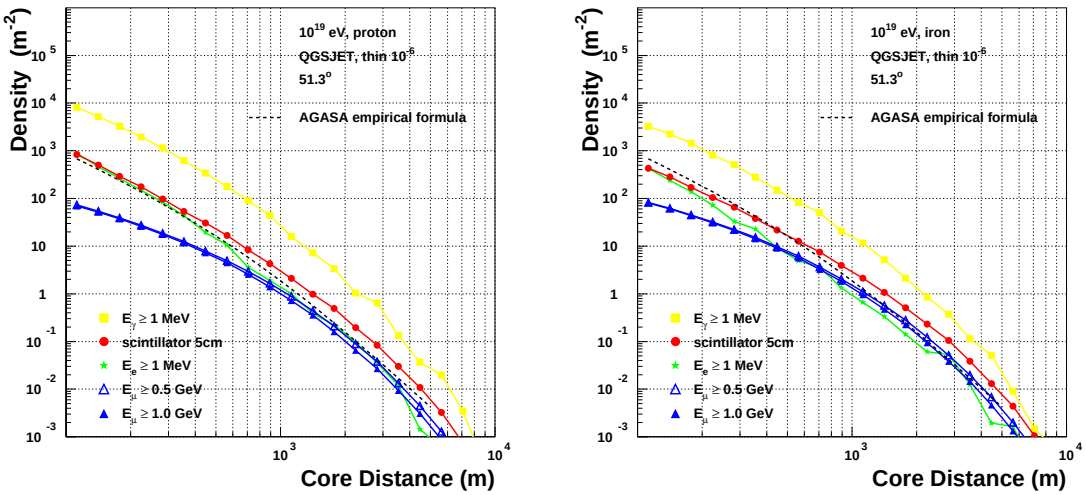

Figure 28: *Same as Fig. 23 except the incident zenith angle of 51.3°. Proton primary (left) and iron primary (right).*

In order to understand the difference, the zenith angle variation of the electron density ($>$ 1 MeV) at 600 m from the core and the muon density (>1 GeV) at 600 m from the core are plotted in Fig. 27. The irregularities in the curves may be due to the statistical fluctuation of the limited number of simulated showers at each point and fitting errors to derive the density at 600 m. Within these uncertainties the *attenuation* with zenith angle by CORSIKA and that by Dai et al. agree with each other as in the left figure of Fig. 27. The difference of abosolute values is partly due to the difference of cutoff energies as described before. Since the number of muons doesn't change with zenith angle and the number of muons in iron initiated showers are larger than that in proton showers as shown in the right figure of Fig. 27, the attenuation of $\rho_{ch}(600)$, which consists of electrons above 1 MeV and muons above 10 MeV, doesn't depend on primary energy and composition.

As is described before, S(600) must be evaluated as $\rho_{sc}(600)$, energy deposit in a scintillator in units of V_{pw}, at various zenith angles taking into account the increase of scintillator thickness with zenith angle. In Fig. 28 the lateral distribution of $\rho_{sc}(600)$ at the zenith angle of 51° is shown. It is found that the energy loss of low energy photons is not important, however, the contribution of muons is significant.

The zenith angle dependence of $\rho_{sc}(600)$ is shown in Fig. 29. As shown in the figure, the attenuation of experimental values is larger that that of iron showers. The difference increases as energy increases. If we take into account the error in $\rho_{ch}(600)$ and zenith angle determination in the experiment, this difference becomes larger as mentioned before. Since the AGASA data have been increased considerably at the highest energy region compared to the one used in the Fig. 29, it may be better to wait further comparisons for the reevaluation of the experimental results.

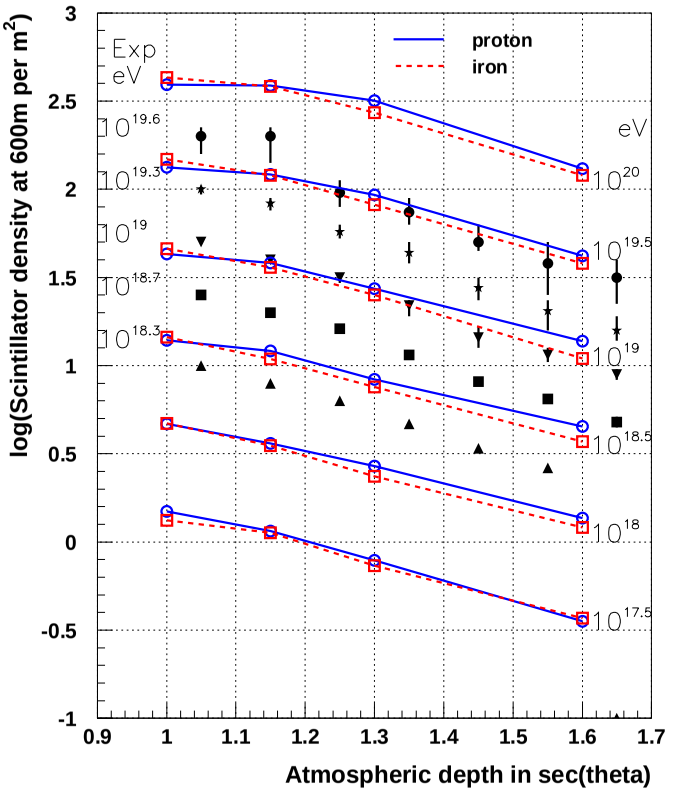

Figure 29: *The variation of $\rho_{sc}(600)$ with zenith angle. Open symbols are from CORSIKA (QGSJET model, thinning level 10^{-6}). Solid lines are from protons and dotted are from iron.*

6 Conclusion

An interpretation of AGASA data has been made by comparing them with results simulated with CORSIKA. Ten air showers for each primariy energies $10^{17.5}$ eV, $10^{18.0}$ eV, $10^{18.5}$ eV, $10^{19.0}$ eV, $10^{19.5}$ eV, and $10^{20.0}$ eV are simulated under each combination of the QGSJET or SIBYLL hadronic models and proton or iron primaries. General features of the electromagnetic component and low energy muons observed by AGASA can be well reproduced by CORSIKA. There are some discrepancies which must be studied in more detail to improve the agreement between the experiment and simulation. In the following some results implicated by the simulation related to the AGASA experiment are summarized.

The form of the lateral distribution of charged particles agrees well with the experimental one between a few hundred m to 2000 m from the core, irrespective of hadronic interaction model or composition and it doesn't depend on the primary energy simulated. Though the shape of muon lateral distibution fits also the ex-

periment, absolute values change with the hadronic interaction model and primary composition.
If we evaluate the density measured by scintillator of 5 cm thickness as S(600) by taking into account similar conditions as in the experiment, the conversion relation from S(600) to the primary energy will be written as

$$E(eV) = (2.95 \pm 0.20) \times 10^{18} \left(\frac{S(600)}{14.25} \right)^{1.015 \pm 0.010}$$

within 10 % uncertainty among models used and composition. This means that the energy assignment of the present AGASA experiment is a lower limit of the CORSIKA energy assignment.
The slope of ρ_μ vs. S(600) relation in the experiment is flatter than that in simulations of any hadronic model and primary composition. The situation may not be changed even by taking into account the primary energy spectrum and fluctuations of ρ_μ and S(600). Since the slope seems to be constant in a wide primary energy range, we need to study this relation in wide primary energy range. Otherwise the composition may be interpreted as heavier than iron or lighter than proton ouside the narrow investigated energy region.
There is a disagreement of the attenuation length determined at AGASA and that by CORSIKA simulation, even if we take into account the particle incident angle to the scintillator. If we take into account the experimental error in zenith angle determination and S(600) determination, the disagreement increases. Since the experimental data is still preliminary, we better wait for the redetermination of experimental values for further discussions.

Acknowledgement

The simulations have been performed by the facilities of the KASCADE group of Institut für Kernphysik III, Forschungszentrum Karlsruhe and the AGASA data published so far are used in this analysis. We acknowledge the kind cooperation of the KASCADE and the AGASA collaborators and Profs. G. Schatz and H. Rebel for valuable comments.
M.N. wishes to thank the Alexander von Humboldt Stiftung and Prof. G. Schatz for their support and warm hospitality during his stay at Karlsruhe. He also wishes to acknowledge all members of the KASCADE group, especially Drs. A. Haungs and K. Bekk, who helped him in performing this study efficiently. He is also grateful to T. Kutter of University of Chicago for his information before the publication and N. Sakaki of ICRR, University of Tokyo who helped him to perform the analysis at the guest house of the University of Karlsruhe.

References

[1] Greisen, K., *Phys. Rev. Letters* **16** 748 (1966), Zatsepin, Z.T. and Kuzmin, V.A., *Pisma Zh. Eksp. Teor. Fiz.* **4** 144 (1966).

[2] Bird, D. et al., *Ap. J.* **441** 144 (1995).

[3] Hayashida, N. et al., *Phys. Rev. Letters* **73** 3491 (1994).

[4] Takeda, M. et al., *Phys. Rev. Letters* **81** 1163 (1998).

[5] Hillas, A.M. et al, *Proc. 12th ICRC (Hobart)* **3** 1001 (1971).

[6] Dai, H.Y. et al., *J. Phys. G: Nucl. Phys.* **14** 793 (1988).

[7] Kasahara, K., Torii, S. and Yuda, T., *Proc. 16th ICRC (Kyoto)* **13** 70 (1979).

[8] Ding, L.K. et al., *Proc. Int. Symp. on Cosmic Rays and Particle Physics* (ed. by T. Yuda, ICRR, Tokyo) 142 (1984).

[9] Nagano, M. et al., *J. Phys. Soc. Japan* **53** 1667 (1984).

[10] Lawrence, M.A. et al., *J. Phys. G: Nucl. Phys.* **17** 733 (1991).

[11] Afanasiev, B.N. et al., *Proc. Tokyo Workshop on Techniques for the Study of the Extremely High Energy Cosmic Rays* (ed. by M. Nagano, ICRR, Tokyo) 35 (1993).

[12] Bird, D.J. et al., *Ap. J.* **424** 491 (1994).

[13] Sakaki, M. et al., *Proc. 25th ICRC (Durban)* **5** 217 (1997).

[14] Cronin, J.W., *GAP-97-034* (Auger Technical Note) (1997).

[15] Kutter, T. and Cronin, J., private communication (1998).

[16] Dawson, B., Meyhandan, R. and Simpson, K.R., *Preprint Astro-ph/9801260* (1998).

[17] Gaisser, T.K. et al., *Phys. Rev. D* **47** 1919 (1993).

[18] Shibata, S. et al., *Proc. 9th ICRC (London)* **2** 672 (1965).

[19] Nagano, M. et al., *J. Phys. G: Nucl. Part. Phys.* **18** 423 (1992).

[20] Hayashida, N. et al., *Proc. 25th ICRC (Durban)* **4** 145 (1997).

[21] Yoshida, S. et al., *J. Phys. G: Nucl. Phys.* **20** 651 (1994).

[22] Heck, D. et al., *FZKA6019* (Forschungszentrum Karlsruhe) (1998).

[23] Knapp, J., Heck, D. and Schatz, G., *FZKA5828* (Forschungszentrum Karlsruhe) (1996).

[24] Heck, D. and Knapp, J., *FZKA6097* (Forschungszentrum Karlsruhe) (1998).

[25] Chiba, N. et al., *Nucl. Instr. and Meth.* **A311** 338 (1992).

[26] Ohoka, H. et al., *Nucl. Instr. and Meth.* **A385** 268 (1996).

[27] Sakaki, N. et al., *in preparation* (1998).

[28] Hayashida, N. et al., *J. Phys. G: Nucl. Phys.* **21** 1101 (1995).

[29] Doi, T. et al., *Proc. 24^{th} ICRC (Rome)* **2** 764 (1995).

[30] Matsubara, Y. et al., *Proc. 19^{th} ICRC (La Jolla)* **7** 119 (1985).

[31] Kalmykov, N.N. and Ostapchenko, S.S., *Yad. Fiz* **56** 105 (1993).

[32] Fletcher, R.S. et al., *Phys. Rev.* **D50** 5710 (1994).

[33] Hillas, A.M., *Proc. Paris Workshop on Cascade Simulation* (ed. by J. Linsley and A.M. Hillas, College Station) 13 (1981).

[34] Greisen, K., Prog. Cosmic Ray Physics, 3^{rd} ed. (ed. by J.G. Wilson) 27 (1956).

[35] Akeno Internal Manual (1980) unpublished.

[36] Teshima, M. et al., *J. Phys. G: Nucl. Phys.* **12** 1097 (1995).

[37] Honda, K. et al., *Phys. Rev. D* **56** 3853 (1997).

[38] Barnett, R.M. et al., *Phys. Rev. D* **54** 1 (1996).

[39] Leibrock, H., Haungs, A. and Rebel, H., *unpublished report* (Forschungszentrum Karlsruhe) (1998).

[40] Shibata, S. et al., *Proc. 9^{th} ICRC (London)* **2** 672 (1965).

[41] Murzin, V.S., *Proc. 9^{th} ICRC (London)* **2** 872 (1965).